© 2021. Published by The Company of Biologists Ltd | Journal of Cell Science (2021) 134, jcs248849. doi:10.1242/jcs.248849

RESEARCH ARTICLE

Mammary mechanobiology – investigating roles for mechanically activated ion channels in lactation and involution

Teneale A. Stewart[1,2], Katherine Hughes[3], Alexander J. Stevenson[1,2], Natascia Marino[4,5], Adler L. Ju[2], Michael Morehead[6] and Felicity M. Davis[1,2,*]

ABSTRACT

The ability of a mother to produce a nutritionally complete neonatal food source has provided a powerful evolutionary advantage to mammals. Milk production by mammary epithelial cells is adaptive, its release is exquisitely timed, and its own glandular stagnation with the permanent cessation of suckling triggers the cell death and tissue remodeling that enables female mammals to nurse successive progeny. Chemical and mechanical signals both play a role in this process. However, despite this duality of input, much remains unknown about the nature and function of mechanical forces in this organ. Here, we characterize the force landscape in the functionally mature gland and the capacity of luminal and basal cells to experience and exert force. We explore molecular instruments for force-sensing, in particular channel-mediated mechanotransduction, revealing increased expression of *Piezo1* in mammary tissue in lactation and confirming functional expression in luminal cells. We also reveal, however, that lactation and involution proceed normally in mice with luminal-specific *Piezo1* deletion. These findings support a multifaceted system of chemical and mechanical sensing in the mammary gland, and a protective redundancy that ensures continued lactational competence and offspring survival.

KEY WORDS: Mammary gland, PIEZO1, Ion channel, Calcium, Lactation, Involution

INTRODUCTION

The adult mouse mammary epithelium consists of an arborized ductal network embedded within an adipose stroma (Macias and Hinck, 2012). The ductal epithelium contains both luminal and basal cells, which are produced and maintained postnatally by lineage-restricted precursors (Davis et al., 2016; Lloyd-Lewis et al., 2017a; Scheele et al., 2017; Sreekumar et al., 2017; Van Keymeulen et al., 2011, 2017). During gestation, a coordinated program of epithelial proliferation, side-branching, differentiation and tissue remodeling takes place (Macias and Hinck, 2012; Zwick et al., 2018), resulting in the generation of thousands of alveolar structures that adorn the central ductal epithelium in lobular clusters (Lloyd-Lewis et al., 2018).

The mammary alveolus is the functional unit of the lactating gland. Within this structure, luminal epithelial cells produce and secrete milk into a central lumen, and surrounding basal epithelial cells contract in response to maternal oxytocin, expelling milk for the suckling neonate (Davis, 2016; Davis et al., 2015; McManaman and Neville, 2003). At the end of lactation, alveolar mammary epithelial cells are removed in one of the largest physiological cell death cascades that occurs postnatally in mammals (Kreuzaler et al., 2011; Sargeant et al., 2014). This returns the mammary epithelium back to a simple ductal tree, enabling further cycles of regeneration, maturation and milk production over the reproductive lifespan of the female (Watson and Kreuzaler, 2011). However, the pregnancy-lactation-involution cycle can permanently alter both mammary epithelial cells and the extracellular matrix composition, a phenomenon that may influence the lifetime risk of tumor development in this organ (dos Santos et al., 2015; Lyons et al., 2011; McDaniel et al., 2006; Meier-Abt et al., 2014; Schedin and Keely, 2011; Schedin et al., 2004; Slepicka et al., 2019).

The formation, function and fate of adult mammary epithelial cells is regulated by a range of local and systemic ligands and their receptors, including progesterone, prolactin, oxytocin and leukemia inhibitory factor (LIF) (Brisken and Ataca, 2015; Gimpl and Fahrenholz, 2001; Kritikou et al., 2003). In addition to the chemical milieu, mammary epithelial cells reside within a complex physical environment, which may regulate tissue condition and function (Nelson and Bissell, 2006; Schedin and Keely, 2011). Mechanical stresses arising from cell-intrinsic forces (e.g. contractile forces generated by the actin-myosin skeleton; Charras and Yap, 2018; Davis et al., 2015; Raymond et al., 2011), cell-extrinsic forces (e.g. epithelial stretching arising from elevated intraluminal pressure; VanHouten et al., 2010) and substrate mechanics (e.g. breast density and tissue tension; Bonnans et al., 2014; Provenzano et al., 2009) are thought to affect cell signaling and function in the mammary epithelium. However, although roles for mechanotransduction in lactation and involution have been proposed (Eisenhoffer et al., 2012; Quaglino et al., 2009; Schedin and Keely, 2011), the magnitude, direction and dynamics of these forces, their mechanisms of reception and transduction, and their physiological roles and redundancies, remain subject to investigation.

Multiple mechanisms exist within cells to detect, decode and transmit force, including integrin-mediated adhesions (Schwartz, 2010) and ion channel-mediated mechanotransduction (or 'mechanoelectrical signaling') (Árnadóttir and Chalfie, 2010; Servin-Vences et al., 2017). In 2010, Piezo channels were identified as bona fide mechanically activated ion channels with important roles in mammalian sensory perception (Coste et al., 2010; Gottlieb, 2017). In non-neuronal tissue, PIEZO1 has been shown to regulate numerous physiological processes ranging from

[1]Mater Research Institute-The University of Queensland, Faculty of Medicine, Woolloongabba, Queensland, 4102, Australia. [2]Translational Research Institute, Woolloongabba, Queensland, 4102, Australia. [3]Department of Veterinary Medicine, University of Cambridge, Cambridge, CB3 0ES, UK. [4]Department of Medicine, Indiana University School of Medicine, Indianapolis, 46202, USA. [5]Susan G. Komen Tissue Bank at Indiana University Simon Cancer Center, Indianapolis, 46202, USA. [6]Lane Department of Computer Science and Electrical Engineering, West Virginia University, Morgantown, 26506, USA.

*Author for correspondence (f.davis@uq.edu.au)

T.A.S., 0000-0003-4837-9315; K.H., 0000-0002-3331-1249; A.J.S., 0000-0001-5909-066X; N.M., 0000-0001-6771-8963; F.M.D., 0000-0001-9112-118X

Handling Editor: Andrew Ewald
Received 12 May 2020; Accepted 6 November 2020

Journal of Cell Science (2021) 134, jcs248849. doi:10.1242/jcs.248849

the maintenance of epithelial barrier integrity (Eisenhoffer et al., 2012; Gudipaty et al., 2017) to lymphatic valve development (Nonomura et al., 2018), red blood cell volume (Cahalan et al., 2015) and myotube formation (Tsuchiya et al., 2018). In the pancreas, PIEZO1 mediates pressure-induced pancreatitis (Romac et al., 2018); however, roles for PIEZO1 channels in the *in vivo* pathophysiology of other exocrine organs, including the mammary gland, remain unexplored (Stewart and Davis, 2019a). Here, we characterize the mammary force landscape and investigate roles for PIEZO1 channels in sensing and transducing epithelial cell forces to sustain or suspend lactation.

RESULTS

Luminal and basal mammary epithelial cells experience repetitive stochastic forces during lactation

The functionally mature mammary epithelium consists of an inner layer of luminal milk-producing cells and an outer layer of basal milk-ejecting cells (Fig. 1A). Differentiated basal cells express smooth muscle contractile proteins, including alpha-smooth muscle actin (SMA) (Haaksma et al., 2011), and contract in response to maternal oxytocin (Davis et al., 2015). To measure the magnitude of basal cell contractions, we engineered mice expressing the red fluorescent protein TdTomato in cytokeratin 5^+ [K5; also known as keratin 5 (KRT5)] basal cells (*TdTomato;K5CreERT2* mice). Using three-dimensional time-lapse imaging of intact mammary tissue pieces from lactating reporter mice, we were able to visualize live basal cells and their thin cellular processes *in situ* at high cellular resolution (Fig. 1B). Quantitative assessment of cell morphology before and after oxytocin stimulation revealed a 32.1±0.8% (mean±s.e.m.; $P<0.05$) decrease in surface area during basal cell contraction (Fig. 1B), making these epithelial cell contractions comparable in magnitude to those of cardiomyocytes and intestinal smooth muscle cells (Stevens and Hunter, 2003; Tokita et al., 2015). To visualize how basal cell-generated forces deform alveolar units for milk expulsion, we loaded mammary tissue from lactating mice with the fluorescent cell-permeable dye CellTracker Red, under conditions that led to the preferential labeling of alveolar luminal cells. These data support stochastic deformations to alveolar structures as a consequence of repetitive basal cell contractions with oxytocin stimulation (Movie 1; Fig. 1C) (21.7±2.8% reduction, Feret's diameter) (Davis et al., 2015; Stevenson et al., 2020).

Milk stasis during involution causes sustained epithelial cell stretching

Post-lactational involution occurs in two stages in mice; the first (reversible) phase (0-48 h), in which return of the offspring can lead to the resumption of lactation; and the second (irreversible) phase (>48 h) marked by alveolar collapse, epithelial cell death and adipocyte regeneration (Fig. 1D) (Hughes et al., 2012; Li et al., 2002; Stein et al., 2007; VanHouten et al., 2010). The first phase of involution is characterized by milk accumulation in the alveolar lumen, resulting in increased intraluminal pressure (Fig. 1D; Fig. S1A) (Hughes et al., 2012; Stein et al., 2007; VanHouten et al., 2010). The sustained overextension of the alveolar epithelium during early involution causes apical cell shedding (Fig. 1D, arrow; Fig. S1A,B) (Lund et al., 1996; Watson, 2006; Watson and Kreuzaler, 2011), a well-established phenomenon that may prolong epithelial barrier integrity by limiting cell density (Eisenhoffer et al., 2012).

Mammary epithelial cells have the potential to sense and respond to extrinsically generated forces arising from the accumulation of milk during post-lactational involution. To quantify the extent and distribution of luminal cell compression experienced during involution, we performed immunohistochemistry (IHC) on mouse mammary tissue. Using E-cadherin immunostaining (to define the basolateral cell membrane) and the fluorescent lectin WGA (to demarcate the apical membrane), we were able to visualize large cellular protrusions extending from the lateral contact sites deep into the alveolar lumen during lactation (Fig. 2A, arrow). Similar apical curvature was observed in lactating human breast tissue (Fig. S1C). Apical projections were absent in tissue samples collected during phase 1 involution (Fig. 2A), suggesting that the apical membrane absorbs a substantial component of the pressure generated through milk stasis. Indeed, luminal cell length and area were reduced by more than 50% by the end of the first phase of involution (Fig. 2B).

Next, we visually inspected luminal cell morphology and volume using serial block face electron microscopy (SBEM). As expected, apical membrane protrusions were visible during lactation (Fig. 2C, asterisks; Movies 2, 3), but absent during early involution (Fig. 2C; Movies 4, 5). Scanning electron microscopy (SEM) of freeze-fractured mammary tissue at different developmental stages enabled visualization of the degree of apical surface distortion during post-lactational involution (Fig. 2D; Fig. S1D) (Pitelka et al., 1973). Consistent with IHC and SBEM imaging, luminal cell length was reduced during involution [Fig. 2D(i) versus D(iv)]. In lactating tissue, microvilli were intact and signs of active secretion were observed [Fig. 2D(ii) and D(iii)]. In contrast, apical surfaces were compressed during involution [Fig. 2D(v) and D(vi)] and microvilli could be observed in endocytic vesicles [Fig. 2D(vi), arrow], consistent with the conversion of these cells to non-professional phagocytes during involution (Hughes et al., 2012; Sargeant et al., 2014). In summary, these data reveal, using a range of techniques for visualization of cell shape and surface characteristics, the changes in luminal cell morphology from lactation to involution. Quantification of cell parameters from IHC experiments confirmed that apical-to-basal length and cell area were reduced during the phase of involution.

Mammary epithelial cells respond to fluid shear stress *in vitro*

To determine how mammary epithelial cells sense force, we first examined intracellular calcium responses in HC11 immortalized mouse mammary epithelial cells in a cell-based fluid flow stimulation assay. HC11 cells treated with lactogenic hormones undergo *in vitro* lactogenic differentiation (Doppler et al., 1989), expressing the lactation markers β-casein (Fig. 3A) and phosphorylated (p)STAT5 (Fig. 3B). The use of the HC11 model overcomes difficulties associated with the culture of primary mammary epithelial cells isolated during the phase of lactation. Non-differentiated (control) and differentiated HC11 cells were loaded with the ratiometric calcium indicator Fura-5F/AM (Xing et al., 2014) and intracellular Ca^{2+} responses to fluid shear stress were examined in real-time using a Molecular Devices ImageXpress Micro high-content imaging system. Using this assay, robotic fluid addition (at a controlled speed and height) inflicts fluid shear stress on HC11 cells cultured on the bottom of the 96-well imaging plate (Xu et al., 2018). A fraction of non-differentiated HC11 cells responded to fluid shear stress via a transient increase in intracellular calcium (ratio of fluorescence at 340 nm to that at 380 nm) (Fig. 3C; Fig. S2A, Movie 6). In contrast, large calcium waves that were propagated from the site of fluid addition were observed in HC11 cells induced to undergo lactogenic differentiation (Fig. 3D,E; Fig. S2A, Movie 6). These data demonstrate that mammary epithelial cells *in vitro* are able to sense force via a pathway that

Journal of Cell Science (2021) 134, jcs248849. doi:10.1242/jcs.248849

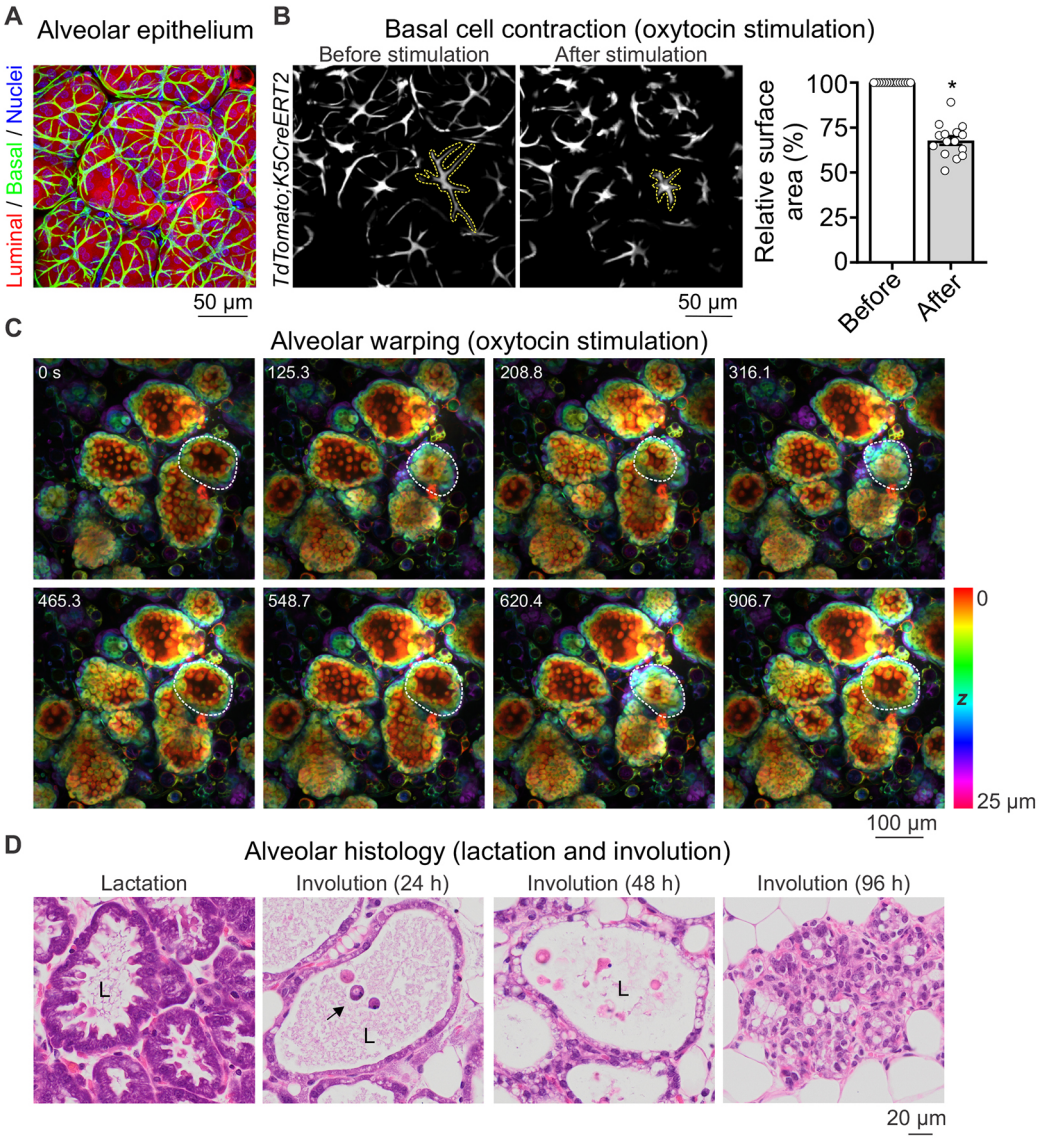

Fig. 1. Mammary epithelial cells experience repetitive stochastic forces during lactation and sustained stretching during early involution. (A) Three-dimensional maximum intensity projection of lactating mammary tissue showing luminal (secretory) epithelial cells stained with CellTracker (red) and basal (contractile) cells with SMA immunostaining (green). Nuclei are blue (DAPI). Representative image from *n*=3 mice. (B) Four-dimensional (*x, y, z, t*) *ex vivo* imaging (see Materials and Methods) of live lactating mammary tissue from *TdTomato;K5CreERT2* reporter mice, showing basal cell surface area before and after oxytocin-mediated cell contraction (85 nM). Dotted-line shows a single tracked cell. Graph shows average relative surface area before and after oxytocin stimulation [mean±s.e.m.; 15 cells (total) from *n*=3 mice, **P*<0.05, unpaired two-tailed Student's *t*-test]. (C) Four-dimensional imaging of live *ex vivo* lactating mammary tissue showing alveolar unit warping due to basal cell-generated force. Tissue was stimulated with oxytocin (85 nM). Dotted line shows a single alveolus through time. Images are depth-coded (see scale bar). See also Movie 1. Representative image stack from *n*=3 mice. (D) Hematoxylin and eosin (H&E) staining of mammary tissue during lactation and involution (24, 48 and 96 h after forced weaning). Arrow shows an apically shed cell; L, alveolar lumen. Representative image from *n*=3 mice at each developmental stage. Further images are shown in Fig. S1A.

involves activation of calcium-permeable ion channel(s). To further explore this in a more physiologically relevant system, we next examined the ion channel 'mechanome' in mouse mammary gland tissue.

Functional PIEZO1 is selectively expressed in luminal epithelial cells

We performed quantitative RT-PCR to examine the expression of putative and established mechanically activated ion channels (Martinac, 2014) in virgin, lactating and involuting mouse mammary tissue (Fig. 4A). RNA samples were validated by β-casein mRNA. Although mRNA for the oxytocin receptor (*Oxtr*) is reported to be enriched in purified basal cells during lactation (Bach et al., 2017), mRNA levels of *Oxtr* and the basal cell marker *Krt14* exhibited a trend to lower expression when examined in lysates prepared from whole tissue (comprised of luminal, basal and stromal cells) (Fig. 4A). This likely reflects the shift in the proportion of basal cells from 33±2.75% (mean±s.e.m.) of total epithelial cells in virgin ducts to 13±1.38% in lactating alveoli (Fig. S2B).

As previously reported (McAndrew et al., 2011; Reinhardt and Horst, 1999), mRNA levels of the calcium ATPase *Pmca2* (also known as *Atp2b2*) and the store-operated calcium entry subunit *Orai1* were significantly enriched in lactating mammary tissue (Fig. 4A). In contrast, gene expression of all transient receptor

Journal of Cell Science (2021) 134, jcs248849. doi:10.1242/jcs.248849

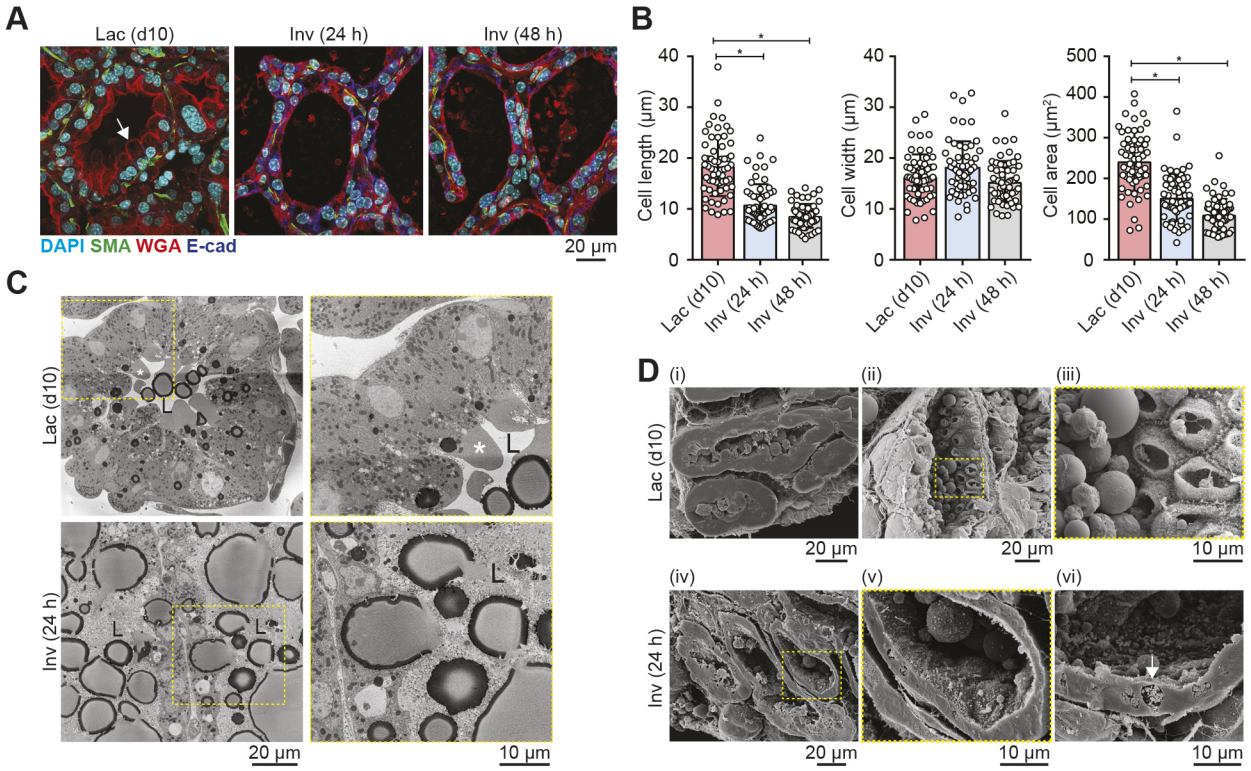

Fig. 2. Intraluminal pressure during mammary gland involution is absorbed by the apical cell membrane of luminal epithelial cells. (A) Representative immunofluorescence staining of lactating (Lac d10) and involuting (Inv, 24 and 48 h) mouse mammary tissue. Immunostaining for SMA reveals basal cells (green) and E-cadherin shows the basolateral membrane of luminal epithelial cells (blue). Apical membranes are stained with WGA (red), nuclei are stained with DAPI (cyan). Arrow shows an apical cell protrusion. Representative of *n*=3 mice at each developmental stage. (B) Quantification of luminal cell length (basal to apical membrane, maximum distance), width (lateral cell junctions, maximum distance) and area. Graphs show mean±s.d.; 60 cells (total) from *n*=3 mice at each developmental stage. **P*<0.05, one-way ANOVA with Bonferroni post-tests. (C) Single slices from SBEM image stacks showing luminal epithelial cells of lactating (Lac d10) and involuting (Inv 24 h) mouse mammary tissue. Boxed region is magnified in adjacent sub-panel; asterisk shows an apical cell protrusion; L, alveolar lumen. See also Movies 2-5. (D) SEM images of freeze-fractured mouse mammary tissue taken from lactating (Lac d10) and involuting (24 h) mice. Boxed region is magnified in subsequent sub-panel; arrow shows endocytic vesicle. Representative images from *n*=3 mice. Further images are shown in Fig. S1D.

potential (TRP) calcium-permeable channels analyzed in this study – the K^+ channels *Trek1* and *Trek2* (also known as *Kcnk2* and *Kcnk10*, respectively) – and the epithelial Na^+ channel *Enac* (also known as *Scnn1g*) were unchanged or were significantly reduced in lactating samples (Fig. 4A). *Trpa1* and *Traak* (also known as *Kcnk4*) transcripts were undetectable in mammary tissue. Reduced expression of ion channels involved in mechanosensory transduction may be a feature of lactogenic differentiation or could be in-part attributable to their lineage-biased expression (as observed with *Oxtr* and *Krt14*). *Piezo1* was the only mechanically activated ion channel examined in this study to exhibit increased expression (2.7±0.58-fold, $P<0.05$) in mammary tissue during lactation (Fig. 4A).

To determine whether PIEZO1 is expressed in both luminal and basal mammary epithelial cell populations, we assessed single-cell calcium responses to the selective PIEZO1 channel activator Yoda1 (Syeda et al., 2015). Primary cells isolated from pregnant mice that express the genetically-encoded calcium indicator GCaMP6f (Chen et al., 2013) in mammary luminal cells (*GCaMP6f;K8CreERT2* mice) showed large, sustained increases in intracellular calcium in response to Yoda1 stimulation (Fig. 4B,C; Movies 7, 8). Yoda1 responses were abolished under extracellular calcium-free conditions, supporting the expression of functional plasmalemmal PIEZO1 channels in mammary luminal epithelial cells (Fig. S3). In contrast, $GCaMP6f^+$ basal cells (isolated from *GCaMP6f-TdTom;K5CreERT2* mice) did not exhibit global increases in cytosolic calcium in response to Yoda1 in single-cell recordings (Fig. 4D,E; Movies 9, 10), but responded, as expected, to stimulation with oxytocin (Stevenson et al., 2020; Stewart and Davis, 2019b). Based on these data, we focused our studies on defining functional roles for PIEZO1 in luminal mammary epithelial cells during lactation and involution.

Luminal PIEZO1 expression is not essential for lactation or involution

To conditionally delete *Piezo1* in luminal epithelial cells, we generated *Piezo1*$^{fl/fl}$*;WAPCre* mice. In this model, Cre-mediated excision occurs downstream of activation of the whey acidic protein (WAP) gene promoter in luminal cells during pregnancy/lactation (Fig. 5A) (Wagner et al., 1997). Female mice were taken through one full pregnancy-lactation-involution cycle and the consequence of genetic deletion of *Piezo1* on mammary gland function was assessed after a second pregnancy (Fig. 5B), at which point more than 90% knockdown of *Piezo1* mRNA was observed (Fig. 5C). Alveologenesis and secretory activation were not altered in *Piezo1*$^{fl/fl}$*;WAPCre* mice (Fig. 5D; Fig. S3B-D). Pups nursed by *Piezo1*$^{fl/fl}$*;WAPCre* mothers gained weight normally (Fig. 5E) and were indistinguishable from pups nursed by control mothers (Fig. 5F), indicating that total milk production and secretion were unaffected by luminal *Piezo1* knockdown.

Advances in our understanding of the molecular mechanisms that enable milk calcium enrichment during lactation have recently been

Journal of Cell Science (2021) 134, jcs248849. doi:10.1242/jcs.248849

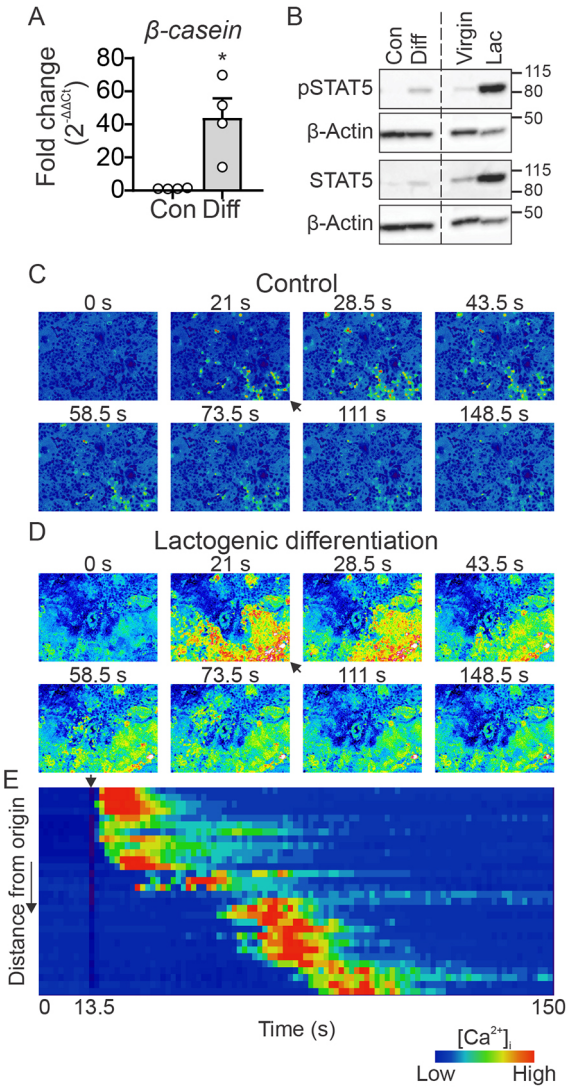

Fig. 3. Mammary epithelial cells respond to fluid shear stress in lactation. (A) HC11 mouse mammary epithelial cells induced to undergo lactogenic differentiation (Diff) express *β-casein* mRNA. Graph shows mean±s.e.m., n=4 independent experiments, *P<0.05, unpaired two-tailed Student's t-test. (B) HC11 mouse mammary epithelial cells induced to undergo lactogenic differentiation have higher levels of activated STAT5 (pSTAT5), as observed in protein lysates from lactating mouse mammary tissue (right). Representative immunoblot (n=4). (C) Non-differentiated (control) HC11 cells stimulated with shear stress (at 15 s) exhibit some transient intracellular calcium responses emanating from the site of fluid addition (black arrow). Images show ratio of fluorescence intensity at 340 nm to 380 nm for Fura-5F. Representative of nine wells from n=3 independent experiments. See also Movie 6 and Fig. S2A. (D) Differentiated HC11 cells stimulated with shear stress (at 15 s) exhibit a large increase in intracellular calcium propagating from the site of fluid addition (arrow). Images show ratio of fluorescence intensity at 340 nm to 380 nm for Fura-5F. (E) Heatmap shows relative intensity (F/F_0, blue to red) of ratioed calcium response as a function of distance from the fluid addition and time. Representative of 9 wells from n=3 independent experiments. See also Movie 6.

made, with the store-operated calcium channel subunit, ORAI1, identified as a major contributor (Davis et al., 2015). The role of other calcium-permeable ion channels (including mechanically activated channels) in this process, however, remains to be elucidated (Montalbetti et al., 2014). It is tempting to speculate that mechanosignaling may help to match milk demand (magnitude and duration of alveolar pumping) with milk composition. However, our study confirmed that milk calcium levels were comparable in control and *Piezo1*$^{fl/fl}$*;WAPCre* mice (Fig. 5G). These data demonstrate that, unlike store-operated channels (Davis et al., 2015), mechanically gated PIEZO1 ion channels are not essential for the basolateral flux of calcium that is required for milk calcium enrichment during lactation (Davis, 2016). Collectively, these data reveal that PIEZO1 channels are either not involved in alveolar morphogenesis, luminal epithelial mechanosensing and milk calcium enrichment during lactation, or they have redundant or compensated roles in these processes. However, our assessment of established and known mechanically activated ion channels in control and *Piezo1*$^{fl/fl}$*;WAPCre* mice revealed no evidence of compensation (at least by channel-mediated mechanotransduction pathways) at the mRNA level (Fig. S4A).

PIEZO1 has also been proposed to regulate cell shedding and death during the early phase of mammary gland involution (Eisenhoffer et al., 2012). Gross morphology of mammary glands stained with the histochemical stain methyl green (Lloyd-Lewis et al., 2016) and analysis of mammary tissue sections showed no discernible differences between control and *Piezo1*$^{fl/fl}$*;WAPCre* mice at either 24 h involution (reversible phase; Fig. 5H) or 72 h involution (irreversible phase; Fig. 5I). The number of cleaved caspase-3$^+$ (CC3$^+$) shed cells was unaffected by luminal *Piezo1* knockdown (Fig. 5J,K; Fig. S4B) (Lloyd-Lewis et al., 2017b). Moreover, luminal cell morphology was unaltered in *Piezo1*$^{fl/fl}$*;WAPCre* mice (Fig. S4C). At the molecular level, conditional deletion of *Piezo1* had no effect on the expression or activation of caspase 7, STAT3 or cathepsin B. We did observe an apparent increase in the expression of the active form of cathepsin L in some tissue samples isolated from *Piezo1*$^{fl/fl}$*;WAPCre* mice during involution (both 24 h and 72 h) (Fig. 5L). However, this difference was not statistically significant (P>0.05, Student's t-test, n=3 independent biological replicates) and activity of this enzyme in tissue lysates was unaltered (Fig. 5M). Finally, we assessed the activity of the calcium-activated proteolytic enzymes calpain-1 and calpain-2. These proteases are induced on weaning (Arnandis et al., 2012) and their activity is diminished in *Piezo1*-null embryos (Li et al., 2014). However, no difference in calpain activity was observed in mammary tissue in this study (Fig. 5N).

Collectively, the data presented here suggest that luminal cell expression of *Piezo1* is not essential for lactation or post-lactational regression. We note, however, that a combination of visual, auditory and tactile sensory inputs are required for the initiation and maintenance of lactation in most mammalian species (Gimpl and Fahrenholz, 2001), and that PIEZO1 channels may have a role in sensing, decoding and transmitting these signals. Moreover, optimal alveologenesis and angiogenesis during gestation depend on cell types that exist outside of the mammary epithelial cell compartment, including tissue macrophages and endothelial cells. Roles for PIEZO1 ion channels in these mammary resident cell types cannot be discounted and should be the subject of future targeted investigations (Fig. S5).

DISCUSSION

The perception and transduction of mechanical signals is ubiquitous in nature. Plants alter their growth and physical form in response to a range of environmental force stimuli, including wind, touch and gravity (Bringmann and Bergmann, 2017). Mechanical inputs guide locomotion in insects (Tuthill and Wilson, 2016). In mammals, mechanosensation underpins fundamental biological processes, ranging from the perception of sound and touch (Pan et al., 2018; Ranade et al., 2014) to the regulation of limb position (Woo et al., 2015) and blood pressure (Zeng et al., 2018). An integrated

Journal of Cell Science (2021) 134, jcs248849. doi:10.1242/jcs.248849

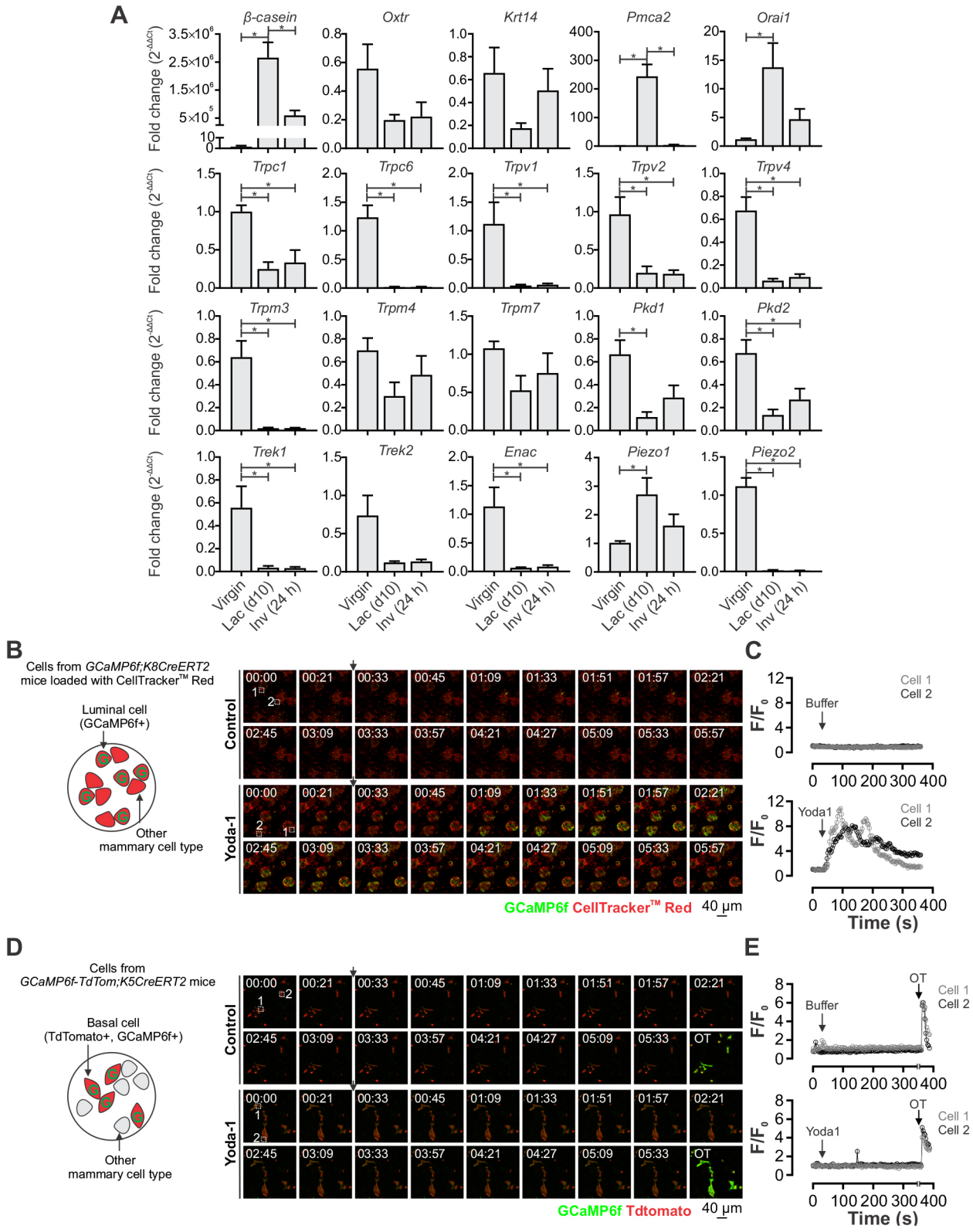

Fig. 4. See next page for legend.

approach to understanding the function and malfunction of tissues in complex multicellular organisms, which incorporates both mechanical and biochemical elements, is therefore essential.

Here, we characterized in greater detail the nature and scale of the mechanical load that mammary epithelial cells experience during lactation and the post-lactational period. These data reveal that, similar to contractile cells in other force-generating organs (Stevens and Hunter, 2003), basal cells in the mammary gland undergo substantial radial shape changes during contraction and relaxation. Using four-dimensional *ex vivo* tissue imaging, we were able to

Fig. 4. Expression of putative and established mechanically activated ion channels in lactation and involution. (A) Assessment of mRNA levels (qRT-PCR) in whole-tissue lysates isolated from virgin, lactating (day 10) and involuting (24 h) mice. Graphs show mean±s.e.m., n=4 mice, *P<0.05, one-way ANOVA with Bonferroni post-tests. mRNA for *Trpa1* and *Traak* were undetectable. (B) Intracellular calcium response to the PIEZO1 channel activator Yoda1 (12 µM) in luminal epithelial cells isolated from pregnant *GCaMP6f;K8CreERT2* mice. Cells were loaded with CellTracker™ (red) for morphology; however, only luminal cells in this mixed mammary cell preparation express the calcium sensor (green). See also Movies 7 and 8. (C) Individual cell traces from two representative cells from each control (buffer only) and Yoda1-stimulated primary luminal cells. (D) Intracellular calcium response to the PIEZO1 channel activator Yoda1 (12 µM) in basal epithelial cells isolated from *GCaMP6f-TdTom;K5CreERT2* mice. In this mixed cell population, basal cells express both TdTomato (red) and the calcium sensor GCaMP6f (green). Cells were stimulated with oxytocin (OT) at the end of the assay to demonstrate their ability to respond. See also Movies 9 and 10. (E) Individual cell traces from two representative cells from each control (buffer only) and Yoda1-stimulated primary basal cells.

demonstrate how this basal cell-mediated force is transmitted to the inner layer of compliant luminal epithelial cells. Finally, we characterized a third form of force in the functionally mature mammary epithelium, which arises as a result of milk accumulation in the alveolar lumen, and were able to visualize, by scanning electron microscopy, the physical footprint of this force on the apical membrane of alveolar luminal epithelial cells.

How mechanical forces are sensed by luminal and basal epithelial cells in the namesake organ of mammals remains an outstanding question in mechanobiology. It is also unclear at this stage whether these forces direct or drive mammary form and function, or whether the tissue develops, functions and remodels despite these mechanical inputs. Our observation that the majority of mammalian mechanically activated ion channels are downregulated during lactation supports the latter theory. In our study, PIEZO1 was the only mechanosensitive ion channel to be upregulated during lactation, at which point stimulation with the specific chemical activator Yoda1 (Syeda et al., 2015), produced an intracellular calcium response in the luminal epithelial lineage. These data suggest that mammary epithelial cells are able to dynamically adapt their mechanosensing machinery in a developmental stage-specific manner to 'channel' mechanoelectrical signaling in lactation through PIEZO1. Of interest, *PIEZO1* has also been shown to be expressed in MCF7 luminal-like breast cancer cells grown *in vitro* (Li et al., 2015), and treatment with GsMTx4, a spider toxin that inhibits PIEZO1, reduces the motility of these cells. Moreover, a separate study has shown that mechanical compression, analogous to that which may occur as a result of cellular overcrowding in the primary tumor, triggers aggressive breast cancer cells to adopt a more invasive phenotype (Tse et al., 2012). Whether breast cancer cells *in vivo* can also dynamically adapt their mechanosensing machinery and upregulate PIEZO1 ion channels, either in response to compressive stress within tumors or in pregnancy associated breast cancer, remains to be determined.

To investigate roles for PIEZO1 in the alveolar epithelium during lactation, we generated a luminal cell-specific *Piezo1* knockout mouse model. In this model, lactation and involution proceeded without major impairment. It is currently unclear what role upregulated and activatable PIEZO1 channels play in the luminal epithelium, whether an as yet unidentified mechanosensitive ion channel or non-channel mechanosignaling protein is able to alter expression and compensate in its absence, or whether inherent biological redundancies exist. Interestingly, although *Piezo1* disruption is embryonic lethal in mice, human patients with homozygous disruption causing generalized lymphatic dysplasia survive into adulthood (Beech and Kalli, 2019; Fotiou et al., 2015). Species-specific differences in the physiological roles of this mechanosensitive ion channel, or in the mechanisms of compensation upon its loss, may exist. In other cell systems, such as stomatal stem cells of *Arabidopsis*, chemical signals are able to override mechanical input to establish cell polarity orientation (Bringmann and Bergmann, 2017). Similar signal duplication with chemical domination may also exist in mammalian cells and systems. Indeed, remarkable redundancy in the creation of the alveolar epithelium by mammary stem/progenitor cells has already been observed in this evolutionarily essential organ (Davis et al., 2016; Lloyd-Lewis et al., 2017a), enabling the mammary gland to fulfil its sole biological role, which is essential for offspring survival in nearly every species in the class Mammalia. The lactating mammary gland, therefore, truly is a 'force' to be reckoned with!

MATERIALS AND METHODS

Reagents

The following reagents were purchased from Sigma Aldrich: RPMI-1640 (R8758), Dulbecco's modified Eagle's medium (DMEM)/F12 (D6434), bovine insulin (I6634), murine epidermal growth factor (E4127), ovine prolactin (L6520), dexamethasone (D4902), collagenase A (11088793001), hyaluronidase (H3506), ammonium chloride (R7757), DNase I (10104159001) and oxytocin (O3251). The following reagents were purchased from Life Technologies: CellTracker Red (C34552), [1,2-bis(o-aminophenoxy)ethane-N,N,N′,N′-tetraacetic acid] (BAPTA) tetrasodium salt (B1214) and DAPI dilactate (D3571). The following kits were purchased from Abcam: cathepsin L Activity Assay (ab65306) and calpain Activity Assay (ab65308). Yoda1 (5586) was purchased from Tocris. Dispase (07913) was purchased from Stem Cell Technologies. MycoAlert Myocoplasma Testing Kit (LT07-218) was purchased from Lonza. Primary and secondary antibody details and dilutions are provided in the histology and immunofluorescence staining or immunoblotting sections. TaqMan Gene Expression assays are provided in Table S1.

Mice

All experimentation was carried out in accordance with the Australian Code for the Care and Use of Animals for Scientific Purposes, the Queensland Animal Care and Protection Act (2001), the National Institutes of Health (NIH) Guide for the Care and Use of Laboratory Animals, the Animal (Scientific Procedures) Act 1986, and the European Union Directive 86/609 with local animal ethics committee approvals. Animals were kept in a specific pathogen free facility, and housed in individually ventilated cages under a 12:12 h light-dark cycle, with water and food available *ad libitum*. The following mice were purchased from The Jackson Laboratory: *WAP-Cre* [B6.Cg-Tg(Wap-cre)11738Mam/JKnwJ, stock number 008735] (Wagner et al., 1997), *Piezo1-flx* (Piezo1$^{tm2.1Apat}$/J, stock number 029213) (Cahalan et al., 2015), *K8-CreERT2* [Tg(Krt8-cre/ERT2)17Blpn/J, stock number 017947] and *K5-CreERT2* [B6N.129S6(Cg)-Krt5$^{tm1.1(cre/ERT2)Blh}$/J, stock number 029155]. *TdTomato-flx* mice were a kind gift from Prof. Ian Frazer (University of Queensland, Australia). *GCaMP6f-flx* mice were a kind gift from Dr. James W. Putney (National Institute of Environmental Health Sciences/NIH). C57BL6/J mice were obtained from the Animal Resources Centre (Western Australia). All strains were acquired and maintained on a C57BL6/J background. *WAP-Cre*, *K8-CreERT2* and *K5-CreERT2* mice were maintained as hemi/heterozygotes. Genotyping was performed on mouse toe, ear or tail DNA by PCR using the following primers: to distinguish Cre positivity in the *WAP-Cre* and *K8-CreERT2* models, 5′-GCGGTCTGGCAGTAAAAACTATC-3′ and 5′-GTGAAACAGCATTGCTGTCACTT-3′ (transgene, 100 bp), and 5′-CTAGGCCACAGAATTGAAAGATCT-3′ and 5′-GTAGGTGGAAATTCTAGCATCATCC-3′ (internal positive control, 324 bp); to distinguish *Piezo1-flx*, 5′-GCCTAGATTCACCTGGCTTC-3′ and 5′-GCTCTTAACCATTGAGCCATCT-3′ (wild type, 188 bp; mutant, 380 bp); to distinguish *K5-CreERT2*, 5′-GCAAGACCCTGGTCCTCAC-3′, 5′-GGAGGAAGTCAGAACCAGGAC-3′ and 5′-ACCGGCCTTATTCCAAGC-3′ (wild type, 322 bp; mutant, 190 bp); to distinguish *TdTomato-flx* and *GCaMP6f-flx*

Journal of Cell Science (2021) 134, jcs248849. doi:10.1242/jcs.248849

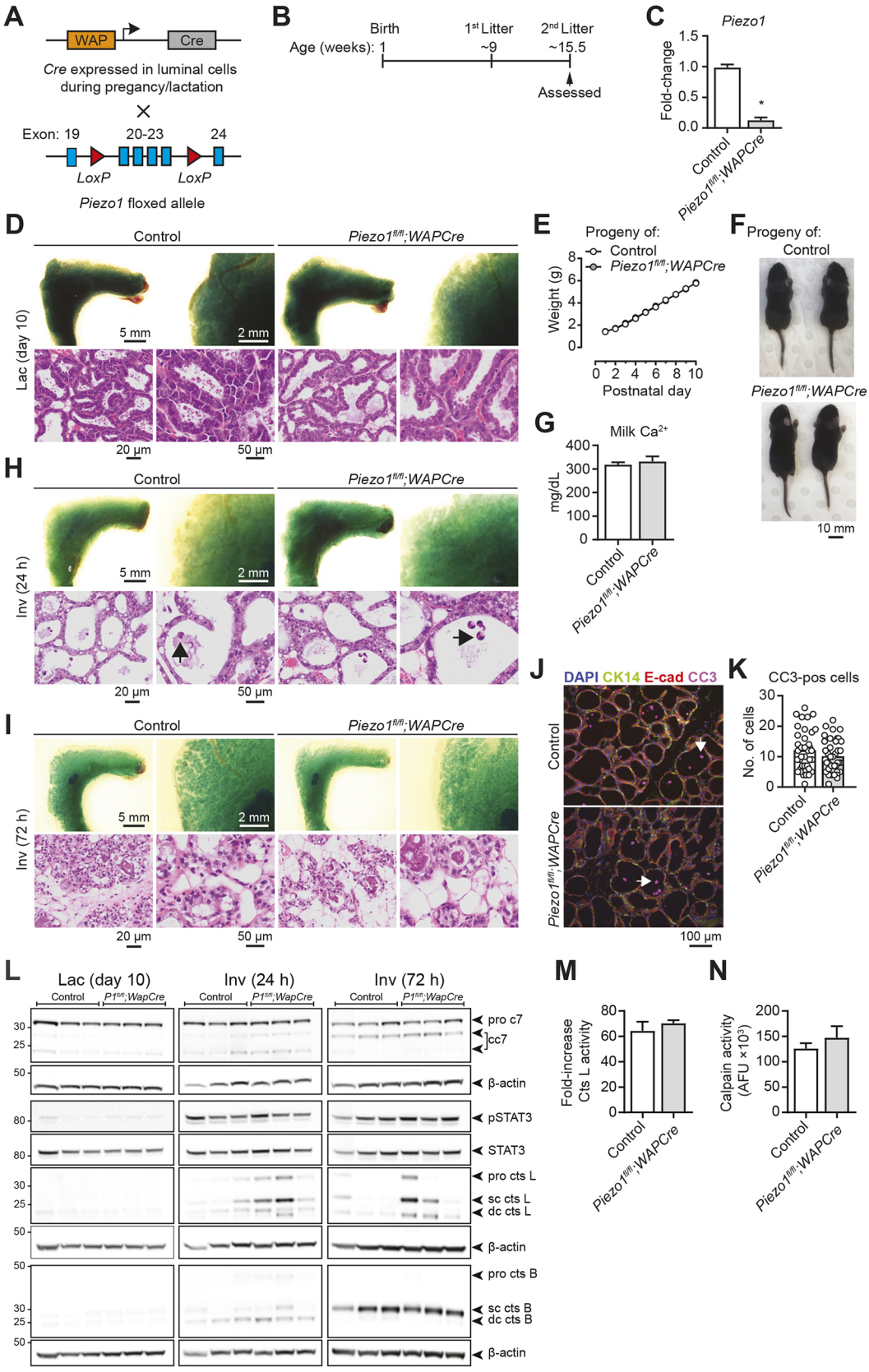

Fig. 5. See next page for legend.

5′-CTCTGCTGCCTCCTGGCTTCT-3′, 5′-CGAGGCGGATCACAAGC-AATA-3′ and 5′-TCAATGGGCGGGGGTCGTT-3′ (wild type, 330 bp; mutant, 250 bp).

To induce recombination in *K5CreERT2* and *K8CreERT2* mice, animals were injected with tamoxifen (1.5 mg) in sunflower oil at 4 weeks of age. A further three tamoxifen injections were administered every second day on

Journal of Cell Science (2021) 134, jcs248849. doi:10.1242/jcs.248849

Fig. 5. Luminal epithelial cell expression of *Piezo1* is not essential for lactation or involution. (A) Schematic representation of the *Piezo1* luminal conditional knockout mouse model. (B) Experimental timeline for *Piezo1$^{fl/fl}$;WAPCre* and control mice. (C) *Piezo1* mRNA levels in control and *Piezo1$^{fl/fl}$;WAPCre* mice (second lactation). Graph shows mean±s.e.m., n=3 mice, *P<0.05, unpaired two-tailed Student's t-test. (D) Mammary gland wholemounts (methyl green) and histology (H&E) show normal alveolar development and secretory activation in lactating (day 10) control and *Piezo1$^{fl/fl}$;WAPCre* mice (second lactation). Representative of n=3 mice from each genotype. (E) Weight gain in pups nursed by control or *Piezo1$^{fl/fl}$;WAPCre* dams from postnatal day (P)1 to P10. Graph shows mean±s.e.m., n=4 mice, P>0.05. (F) Representative images (n=3 litters per genotype) of pups born to and nursed by control or *Piezo1$^{fl/fl}$;WAPCre* mice. (G) Milk calcium concentrations in control and *Piezo1$^{fl/fl}$;WAPCre* mice. Graph shows mean±s.e.m., n=3 mice, P>0.05, unpaired two-tailed Student's t-test. (H) Wholemounts (methyl green) and histology (H&E) of control and Piezo1fl/fl;WAPCre mouse mammary tissue 24 h after forced weaning (second lactation). Representative of n=4 mice of each genotype. (I) Wholemounts (methyl green) and histology (H&E) of control and *Piezo1$^{fl/fl}$;WAPCre* mouse mammary tissue 72 h after forced weaning (second lactation). Representative of n=3 (wholemount) or n=6 (H&E) mice of each genotype. (J) Immunofluorescence staining for cleaved caspase 3 (CC3, magenta), E-cadherin (red) and K14 (green) at 24 h involution. Nuclei are stained with DAPI (blue). Representative images from n=4 mice of each genotype. Arrows show CC3 positive apically shed cells. Further images are shown in Fig. S4B. (K) Quantification of the number of apically shed cells in control and *Piezo1$^{fl/fl}$;WAPCre* at 24 h involution. Graph shows mean±s.e.m. from 37-40 fields of view (total) averaged from n=4 mice, P>0.05, unpaired two-tailed Student's t-test. (L) Western blot analysis of whole-tissue lysates from lactating (day 10) and involuting (24 h and 72 h) control and *Piezo1$^{fl/fl}$;WAPCre* mice showing pro- and cleaved caspase 7 (pro c7 and cc7, respectively), total and active STAT3 (STAT3 and pSTAT3, respectively), and cathepsins L and B (cts L, B; pro sc, single chain and dc, heavy chain of the double-chain form); n=3 independent biological replicates. (M) Cathepsin L (cts L) activity in whole-tissue lysates from control and *Piezo1$^{fl/fl}$;WAPCre* mice during involution (72 h). Activity is displayed as fold-increase relative to the negative control. Graph shows mean±s.e.m., n=3 independent biological replicates, P>0.05, unpaired two-tailed Student's t-test. (N) Calpain activity [shown as arbitrary fluorescence units (AFU)] in whole-tissue lysates from control and *Piezo1$^{fl/fl}$;WAPCre* mice during involution (72 h). Graph shows mean±s.e.m., n=6 independent biological replicates, P>0.05, unpaired two-tailed Student's t-test.

alternating sides at 8 weeks of age (total dose, 6 mg). The dose and timing of tamoxifen administration (1.5 mg at the onset of puberty) had little effect on ductal morphogenesis (Rios et al., 2014) and resulted in 95.7±1.6% recombination in basal cells (measured by fluorescent reporter expression) (Stevenson et al., 2020). Mice were taken through a 6-week washout before mating. To induce recombination in *WAPCre* mice, animals were taken through one full pregnancy-lactation-involution cycle. Pups (average 8; range 6-10) were weaned on postnatal day (P)21. Mothers were mated 1 week later in their second (experimental) mating. For all experimental litters, pup number was standardized to six to eight.

To obtain tissue during lactation and involution, adult female mice were mated with C57BL6/J sires and allowed to litter naturally. Lactating tissue was harvested on day 10 of lactation. For forced involution studies, pups were removed on day 10 of lactation (range 10-12) and tissue was harvested from involuting mothers 24, 72, or 96 h later, as indicated (Stewart and Davis, 2020).

Cell lines

HC11 cells (originally isolated from the mammary gland of a pregnant mouse) (Hynes et al., 2015) were a gift from Prof. Melissa Brown (The University of Queensland, Australia). Cells were maintained in RPMI 1640 medium with L-glutamine and sodium bicarbonate (R8758, Sigma-Aldrich), supplemented with 10% fetal bovine serum (FBS; Thermo Fisher Scientific), bovine insulin (5 µg/ml, I6634, Sigma-Aldrich) and murine epidermal growth factor (10 ng/ml, E4127, Sigma-Aldrich). To induce differentiation, HC11 cells were first cultured for 48 h in maintenance media, followed by 24 h in pre-differentiation media containing RPMI-1640, FBS (10%) and bovine insulin (5 µg/ml). Cells were grown for a further 96 h in differentiation media containing RPMI-1640, FBS (10%), bovine insulin (5 µg/ml), ovine prolactin (5 µg/ml, L6520, Sigma-Aldrich) and dexamethasone (1 µM, D4902, Sigma-Aldrich), with daily media changes. HC11 cells were maintained in a humidified incubator at 37°C with 5% CO_2, and routinely (every 6 months) tested negative for mycoplasma (MycoAlert, LT07-218, Lonza).

Human subjects

Breast tissue biopsies from lactating women, who showed no evidence of breast cancer at the time of donation, were obtained from the Susan G. Komen Tissue Bank at the Indiana University Simon Cancer Center, USA (www.komentissuebank.iu.edu/) (Sherman et al., 2012). All samples were obtained with informed consent, and patients (females aged 25-42) were recruited under a protocol approved by the Indiana University Institutional Review Board (IRB protocol number 1011003097) and according to The Code of Ethics of the World Medical Association (Declaration of Helsinki). The current project received additional site-specific approval from the Mater Misericordiae Ltd Human Research Ethics Committee. Tissue was formalin fixed and paraffin embedded, as per standard protocols. Women classified as lactating had at least one live birth (range 1-4) and were actively breastfeeding at the time of tissue donation (at least once daily).

Live-cell imaging

HC11 fluid sheer stress calcium imaging experiments were performed in physiological salt solution (PSS; 10 mM HEPES, 5.9 mM KCl, 1.4 mM $MgCl_2$, 1.2 mM NaH_2PO_4, 5 mM $NaHCO_3$, 140 mM NaCl, 11.5 mM glucose and 1.8 mM $CaCl_2$; pH 7.3-7.4). For fluid shear stress experiments, HC11 cells were plated in 96-well optical-grade TC-treated black microplates (353219, BD Biosciences) and differentiated (as indicated), as described above. HC11 cells were loaded with the ratiometric calcium indicator Fura-5F/AM (4 µM, 6616, Setareh Biotech) for 30 min at 37°C. Excess dye was removed by washing in PSS-Ca^{2+}, containing bovine serum albumin (0.3%), and then PSS-Ca^{2+}, before being allowed to settle for ∼5 min before imaging. Cells were bathed in 100 µl of PSS-Ca^{2+} and were 'stimulated' by the addition of 100 µl of PSS-Ca^{2+} at a 90° angle below the liquid-air interface at a defined rate of 200 µl s^{-1} using an ImageXpress Micro XLS widefield high-content system with fluidic control (Molecular Devices) (Bassett et al., 2018). In this assay, the moving fluid, dispensed close to the cell monolayer over 500 ms, imposes transient flow stimulus on cells at the bottom of the well. Images were recorded every 1.5 s for 150 s using a 10× Plan Fluor objective. The ImageJ custom built plug-in Ratio Plus (Rudolf et al., 2006) was used to create 340/380 ratios. The Time Series Analyzer (v3) plugin was used to create 30 regions of interest diagonally from the determined origin of the shear stress stimulus. Starting fluorescence (F_0) was calculated by averaging the intensity ratios for the first four frames before stimulation. A heatplot of fluorescence intensity (F/F_0) through time (x) as a function of distance from the origin of the shear stress stimulus (y) was generated using the Heatmapper web server developed and published by Babicki et al. (2016).

For live imaging of primary cells isolated from *GCaMP6f;K8CreERT2* and *GCaMP6f-tdTom;K5CreERT2* mice, tissue was removed and cells dissociated as described previously (Prater et al., 2013) with minor changes. Briefly, tissue was finely minced and incubated in DMEM/Ham's F12 (D6434, Sigma-Aldrich) containing collagenase (1 mg/ml, 11088793001, Roche) and hyaluronidase (100 U/ml, H3506, Sigma-Aldrich), at 37°C with gentle rocking for 3 h. The cell slurry was broken up further by pipetting with a sterile transfer pipette every 30 min. The cell slurry was then centrifuged at 1500 rpm for 5 min at 4°C, and the cell pellet was resuspended in dissociation buffer (Hank's balanced salt solution with 2% FBS). Red blood cell lysis was performed using ammonium chloride solution (R7757, Sigma-Aldrich). The cell suspension in dissociation buffer was treated with trypsin (0.25%) for 1 min, then treated with dispase (5 mg/ml, 07913, Stem Cell Technologies) and DNase (1 mg/ml, 10104159001, Sigma-Aldrich), strained through a 40 µm cell strainer and plated on collagen-coated (50 µg/ml) optical-grade imaging plates in DMEM/F12 containing FBS (10%) and gentamycin (50 µg/ml, G1272, Sigma-Aldrich). Following dissociation, cells were left to attach for at least 3 h in a humidified incubator at 37°C with 5% CO_2. *GCaMP6f;K8CreERT2*

primary cells were loaded with CellTracker Red (1 µM, C34552, Life Technologies) in DMEM/F12 containing 10% FBS and gentamycin (50 µg/ml) for at least 30 min at 37°C before imaging. Primary cells were imaged in DMEM/F12 containing 10% FCS and gentamycin (50 µg/ml), and were stimulated with either PSS-Ca^{2+} or Yoda1 (12 µM final, 5586, Tocris) in PSS-Ca^{2+}. For extracellular calcium-free experiments, cells were imaged in calcium-free PSS (supplemented with 500 µM BAPTA) and stimulated with Yoda1 (final concentration 15 µM). For studies assessing responses under physiological calcium concentrations, cells were bathed in PSS-Ca^{2+} and stimulated with either buffer (PSS-Ca^{2+}) or Yoda1 (final concentration 15 µM). Images were acquired using an Olympus FV3000 inverted confocal microscope with a UPLSAPO 30×/1.05 silicone objective, resonant scanner and a z-drift compensator (ZDC).

Ex vivo four-dimensional tissue imaging

Live three-dimensional time-lapse (4D) imaging was performed as described previously (Davis et al., 2015). Briefly, mammary tissue was harvested from lactating dams, diced into 3-5 mm^3 pieces and loaded with CellTracker Red (1.5 µM) in DMEM containing 10% FBS for at least 20 min at 37°C. Tissue was imaged in a glass bottom (1.5) 35 mm µ-dish (Ibidi) using anchored inert netting to loosely secure the tissue in position. Tissue was bathed in PSS-Ca^{2+} and stimulated with oxytocin (85 nM, O3251, Sigma-Aldrich) in PSS-Ca^{2+}.

Mouse milking

For mouse milking studies, lactating dams were removed from the nest for 2 h before milking on lactation day 5. Lactating mice were lightly anesthetized using isoflurane (2%). Mice were administered oxytocin (2 IU) by intraperitoneal injection, and milking from the right abdominal mammary gland was initiated 2 min later. Milk was discharged by light manual manipulation of the mammary gland and was immediately collected from the tip of the nipple using a pipette (Stewart and Davis, 2020).

Milk Ca^{2+} measurements

Free calcium concentrations in mouse milk were determined using a phenolsulphonephthalein reaction with a QuantiChrom Calcium Assay Kit (DICA-500, BioAssay Systems) as per the manufacturer's instructions and as previously reported in mouse milk samples (Davis et al., 2015).

Histology and immunofluorescence staining

Mouse tissue was dissected, spread on biopsy pads and fixed in neutral buffered formalin (NBF, 10%) overnight at room temperature. Routine processing and paraffin embedding was performed by immersion in 70% ethanol (45 min), 90% ethanol (45 min), 95% ethanol (45 min), 100% ethanol (45 min, three times), xylene (30 min, three times) and then paraffin (1 h, 60°C, three times) (Stewart and Davis, 2020). Formalin-fixed paraffin-embedded (FFPE) slides were cut to 4-5 µm. Immunofluorescence staining was performed by heat-induced epitope retrieval, as described previously (Davis et al., 2016). Briefly, FFPE slides were deparaffinized by immersion in xylene (3 times for 5 min each time) and rehydrated through a reducing ethanol series. Permeabilization was performed by immersion in PBS containing Triton X-100 (0.5%). Antigen retrieval in sodium citrate buffer (0.01 M, pH 6) was performed using a Decloaking Chamber NxGen digital pressure system (Biocare Medical) at 110°C for 11 min. Tissue sections were blocked for 1 h in normal goat serum (10%) in PBS containing Triton X-100 (0.05%). Primary antibody incubation was performed overnight in a humidified chamber at 4°C. Secondary antibody incubation (1:500) and wheat germ agglutinin (WGA; 5 µg/ml) staining was performed for 1 h at room temperature. Nuclear DAPI (625 ng/ml) staining was performed for 10 min at room temperature (Stewart and Davis, 2020). The following primary antibodies and dilutions were used in this study: rabbit anti-SMA (ab5694, Abcam, 1:400-800), rabbit anti-E-cadherin (3195S, Cell Signaling Technology, 1:400), mouse anti-E-cadherin (610182, BD Biosciences, 1:200), rabbit anti-CC3 (9611, Cell Signaling Technology, 1:200), chicken anti-K14 (906004, BioLegend, 1:200), anti-rabbit PGP9.5 (108986, Abcam, 1:100) and rabbit anti-PMCA2 (P1244, Sigma-Aldrich, 1:200). The following secondary antibodies were used: goat anti-mouse IgG Alexa Fluor 647 (A21236, Life Technologies), goat anti-rabbit IgG Alexa Fluor 647 (A21245, Life Technologies), goat anti-mouse IgG Alexa Fluor 555 (A32727, Life Technologies), goat anti-mouse IgG Alexa Fluor 488 (A11001, Life Technologies), goat anti-rabbit IgG Alexa Fluor 488 (A32731, Life Technologies) and goat anti-chicken IgG Alexa Fluor 488 (11093, Life Technologies). Sections were imaged using an Olympus BX63F upright epifluorescent microscope with UPlanSAPO 10×/0.4, 20×/0.75, 40×/0.95, 60×/1.35 and 100×/1.35 objective lenses. Hematoxylin and eosin (H&E)-stained slides were imaged on an Olympus VS120-L100-W Slide Scanner. Rabbit mammary tissue was collected and fixed in NBF (10%), processed and sectioned at 5 µm, as previously described (Hughes and Watson, 2018). H&E staining was performed using standard histological protocols.

CUBIC tissue clearing and whole-mount immunostaining

Mammary tissue was dissected and fixed for 6 to 9 h, as previously optimized for whole-mount immunostaining in the mammary gland (Lloyd-Lewis et al., 2016, 2018). Tissue clearing was performed using a modified CUBIC protocol (CUBIC 1A) (Lloyd-Lewis et al., 2016; Susaki and Ueda, 2016) or SeeDB (Ke et al., 2013). Whole-mount immunostaining was performed following immersion in CUBIC Reagent 1A for 1 to 3 days (depending on tissue size) and overnight blocking in PBS with normal goat serum (10%) and Triton X-100 (0.5%) (Lloyd-Lewis et al., 2016). SeeDB immersion clearing was performed as described previously (Davis et al., 2016). The following primary antibodies were used: anti-rabbit SMA (1:300) and anti-PGP9.5 (1:150). DAPI (5 µg/ml) staining was performed at room temperature for 2 h. For imaging CellTracker in cleared mammary tissue, tissue was loaded with CellTracker Red (1.5 µM) in complete medium for 30 min before fixing. All tissue cleared using the CUBIC protocol was immersed in CUBIC Reagent 2 for at least 24 h before imaging. Cleared and immunostained tissue was imaged using an Olympus FV3000 laser scanning confocal microscope with UPLSAPO 10×/0.40, UPLSAPO 20×/0.75, UPLSAPO 30×/1.05 and UPLFLN 40×/0.75 objective lenses. Visualization and image processing was performed in ImageJ (v1.52e, National Institutes of Health) (Linkert et al., 2010; Schindelin et al., 2012). Denoising of three-dimensional image sequences was performed as described previously (Boulanger et al., 2010).

Whole-mount histochemistry

Intact abdominal and inguinal mammary glands were dissected, spread on Tetra-Pak card and fixed overnight in 10% NBF at room temperature. Fixed tissue was immersed in CUBIC reagent 1 for 3 days at 37°C and then placed in methyl green (0.5%) for 1.5 h (Stewart and Davis, 2020). Following staining, tissue was rinsed twice in tap water and once in distilled water before de-staining for 20 min in acid alcohol [50% ethanol and HCl (25 mM)]. After de-staining, tissue was transferred to CUBIC reagent 2 for 24 h and imaged using an Olympus SZX10 stereo microscope with a DF PLAPO 1× objective.

Real-time RT-PCR

For RNA isolation from HC11 cell cultures, cells were lysed in Qiagen Buffer RLT Plus. For RNA isolation from mouse mammary tissue, tissue was dissected from the abdominal mammary gland of virgin, lactating (day 10) and involuting (24 h) mice, and immediately snap frozen in liquid nitrogen (Stewart and Davis, 2020). Frozen tissue pieces (50-100 mg) were crushed using a mortar and pestle, resuspended in Qiagen Buffer RLT Plus and homogenized using QIAshredder homogenizer columns (79651, Qiagen). RNA was isolated and purified using the RNeasy Plus Mini Kit with gDNA Eliminator columns (74134, Qiagen). Reverse transcription was performed using the QuantiTect Reverse Transcription Kit with integrated removal of genomic DNA contamination (205311, Qiagen), and resulting cDNA was amplified using an Applied Biosystems ViiA 7 Real-time PCR System, using TaqMan Fast Universal PCR Master Mix (4352042, Applied Biosystems) and TaqMan Gene Expression Assays (Applied Biosystems) (see Table S1). Relative quantification was calculated with reference to 18S ribosomal RNA and analysed using the comparative C_T method (Suchanek et al., 2002).

Immunoblotting

HC11 total cellular protein was isolated using protein lysis buffer [100 mM NaCl, 50 mM Tris base pH 8.0, 1% IGEPAL CA-630 (I3021,

Sigma-Aldrich), 0.5% (w/v) sodium deoxycholate (D6750, Sigma-Aldrich)] supplemented with protease and phosphatase inhibitors (A32959, Thermo Fisher Scientific), and immunoblotting was performed as described previously (Davis et al., 2014). The following primary antibodies were used in this study: mouse anti-β-actin (A5441, Sigma-Aldrich, 1:10,000), rabbit phospho-STAT5 (4322, Cell Signaling Technology, 1:1000), and mouse anti-STAT5 (sc-74442, Santa Cruz Biotechnology, 1:500). Samples were incubated with these antibodies at 4°C overnight. The following secondary antibodies were used: goat anti-mouse IgG horseradish peroxidase (HRP) conjugate (170-6516, Bio-Rad, 1:10,000) and goat anti-rabbit IgG HRP conjugate (170-6515, Bio-Rad, 1:10,000). Samples were incubated with these antibodies for 1 h at room temperature. Images were acquired using a Fusion SL chemiluminescence imaging system (Vilber Lourmat).

For total protein isolation from mouse mammary tissue, tissue was dissected from the abdominal mammary gland of lactating (day 10) and involuting (24 h and 72 h) mice, and immediately snap frozen in liquid nitrogen. Frozen tissue pieces (50-100 mg) were crushed using a mortar and pestle, and homogenized in protein lysis buffer supplemented with protease and phosphatase inhibitors. Protein concentration was estimated by Bradford Assay (5000006, Bio-Rad) and immunoblotting was performed as described previously (Davis et al., 2014). The following primary antibodies were used: mouse anti-β-actin (AC-15) (A5441, Sigma-Aldrich, 1:10,000), rabbit anti-caspase 7 (9492, Cell Signaling Technology, 1:1000), rat anti-cathepsin L (MAB9592, R&D Systems, 1:1000), rat anti-cathepsin B (MAB965, R&D Systems, 1:1000), mouse anti-STAT3 (124H6) (9139, Cell Signaling Technology, 1:1000) and rabbit anti-pSTAT3 (Tyr705) (9145, Cell Signaling Technology, 1:1000). Samples were incubated with these antibodies at 4°C overnight. The following secondary antibodies were used: goat anti-mouse IgG HRP conjugate (170-6516, Bio-Rad, 1:10,000), goat anti-rabbit IgG HRP conjugate (170-6515, Bio-Rad, 1:10,000) and goat anti-rat IgG HRP conjugate (ab205720, Abcam, 1:10,000). Samples were incubated with these antibodies for 1 h at room temperature. Images were acquired using a Fusion SL chemiluminescence imaging system (Vilber Lourmat). Densitometry was performed using ImageJ.

Enzyme activity assays

Assessment of cathepsin L and calpain activity in fresh frozen mammary tissue was performed using commercial kits (ab65306, Abcam and ab65308, Abcam, respectively). Lysates were prepared according to the manufacturer's instructions. Calpain assay inputs were standardized according to total protein concentration, as per the manufacturer's instructions. Cathepsin L activity is based on the cleavage of the synthetic substrate Ac-FR-AFC to free amino-4-trifluoromethyl coumarin (AFC). Calpain activity is based on the cleavage of the synthetic substrate Ac-LLY-AFC to free AFC. AFC fluorescence was detected using a PHERAstar FS microplate reader (BMG LabTech) equipped with a 400 nm excitation filter and 500 nm emission filter. Activity was calculated as indicated in the figure legend following subtraction of background.

Electron microscopy

For electron microscopy studies, animals were euthanized and on confirmation of death, abdominal and inguinal mammary glands were immediately harvested and processed into ∼3 mm^3 pieces in the presence of fixative containing glutaraldehyde (2.5%) and formaldehyde (3%) in cacodylate. For serial block-face electron microscopy (SBEM), samples were processed using a PELCO BioWave microwave (Ted Pella) as per Webb and Schieber (2018), according to the microwave processing protocol. Samples were imaged and sectioned using a Zeiss Sigma scanning electron microscope fitted with a 3View (Gatan) at 2 kV (involution 24 h) or 3 kV (lactation d10). The resultant SBEM images were aligned using the StackReg ImageJ plug-in (Thévenaz et al., 1998), and image segmentation was performed semi-automatically via the Ilastik segmentation toolkit carving workflow (Sommer et al., 2011). Image segmentation was further proofed and corrected using the Seg3D open-source software package (NIH/NIGMS Center for Integrative Biomedical Computing). SBEM movies were created in virtual reality using syGlass (Pidhorskyi et al., 2018 preprint).

For scanning electron microscopy (SEM), samples were post-fixed in osmium tetroxide (1%) and dehydrated in an ethanol series before being dried in an Autosamdri critical point dryer (Tousimis). Samples were freeze-fractured in liquid nitrogen before mounting on SEM pin mounts (G0404, ProSciTech) and gold-coated in a sputter coater (SPI). Images were acquired using a JCM-5000 NeoScope (Jeol) at 10 kV.

Analysis of basal cell contraction and alveolar unit warping

Basal cell surface area was analyzed using the surface tool in Imaris 9.2.1 (Bitplane). Cells were selected based on intensity and visibility in the field of view (five cells per animal) and surface area for each cell measured before oxytocin stimulation (range 3.25-19.54s) and at maximal contraction post-oxytocin stimulation (range 104-472.27s). To determine alveolar warping, we created maximum intensity *z*-projections in ImageJ from image sequences of alveolar units loaded with CellTracker Red. We manually traced the perimeter of three alveolar units (selected based on visibility within the field of view) from each animal before oxytocin stimulation and at maximal contraction post-oxytocin (85 nM) stimulation. Feret's diameter was calculated using ImageJ.

Luminal cell size measurements

Luminal cell length (basal to apical, maximum distance), width (lateral, widest point) and area were calculated in FIJI using the straight line and freehand drawing tools, and measure function.

Histological analyses

Quantification of the number of shed cells was performed on mammary tissue sections (H&E staining) at lactation day 10, and involution (24 h and 48 h), based on morphological characteristics (highly condensed nuclei and swollen appearance of cells) (Lund et al., 1996; Watson, 2006; Watson and Kreuzaler, 2011). Histological sections of mammary tissue from control and *Piezo1*$^{fl/fl}$*;WAPCre* mice were analyzed by an American College of Veterinary Pathologists board certified pathologist experienced in mouse mammary histopathology and blinded to mouse genotype. Evaluation used whole slide images and digital microscopy. Histological assessment included all aspects of glandular morphology, including consideration of both the epithelial and stromal compartments, taking into account the proportion of alveolar units, the degree of expansion/collapse of alveolar units, lumen size, epithelial cell morphology and degree of adipocyte infiltration.

Relative stromal (non-alveolar tissue) area and lumen (ductal and alveolar) area of representative H&E-stained lactating (day 10) mammary tissue sections from control and *Piezo1*$^{fl/fl}$*;WAPCre* dams (second lactation) were quantified in FIJI using area selection tools and the measure function. The ratio of either stromal or lumen area was calculated by dividing the sum of either stromal or lumen areas by total tissue area. Results are expressed as the percentage of total tissue area.

Statistical analysis

Statistical analysis was performed using GraphPad Prism (v7.03). Statistical tests are detailed in the figure legends. All statistical analyses were performed using the average value for each independent repeat, where n=3 to 6 mice, as indicated.

Acknowledgements

The authors acknowledge the Translational Research Institute (TRI) for the research space, equipment and core facilities that enabled this research. We thank the University of Queensland Biological Resource Facility staff for help with animal work; Dr Corinne Alberthsen for assistance with research ethics applications and compliance; Mr Richard Webb, Ms Robyn Chapman and Dr Kathryn Green (Centre for Microscopy and Microanalysis) for their support with the electron microscopy studies; Dr Jerome Boulanger (Medical Research Council Laboratory of Molecular Biology) for the 3D denoising algorithm; and Dr Adam Ewing and Mr Eric Pizzani (TRI) for research computing support. Samples from the Susan G. Komen Tissue Bank at the Indiana University Simon Cancer Center were used in this study; we thank contributors, including Indiana University (sample collection), as well as donors and their families.

Competing interests

M.M. is Chief Executive Officer at IstoVisio, Inc. and co-creator of syGlass (IstoVisio), the visualization software used to prepare Movies 2, 3, 4 and 5.

Author contributions
Conceptualization: T.A.S., F.M.D.; Methodology: T.A.S., F.M.D.; Formal analysis: T.A.S., K.H., A.J.S., A.L.J., F.M.D.; Investigation: T.A.S., K.H., A.J.S., F.M.D.; Resources: N.M., F.M.D.; Writing - original draft: T.A.S., F.M.D.; Writing - review & editing: T.A.S., F.M.D.; Visualization: T.A.S., A.L.J., M.M., F.M.D.; Supervision: F.M.D.; Project administration: F.M.D.; Funding acquisition: F.M.D.

Funding
This work was supported by the National Health and Medical Research Council of Australia (1141008 and 1138214 to F.M.D.), National Stem Cell Foundation of Australia (Metcalf Award to F.M.D.), the University of Queensland (Foundation Research Excellence Award to F.M.D.), and the Mater Foundation (Equity Trustees/ A.E. Hingeley Trust to F.M.D.).

Supplementary information
Supplementary information available online at
https://jcs.biologists.org/lookup/doi/10.1242/jcs.248849.supplemental

Peer review history
The peer review history is available at
https://dev.biologists.org/lookup/doi/10.1242/jcs.248849.reviewer-comments.pdf

References

Árnadóttir, J. and Chalfie, M. (2010). Eukaryotic mechanosensitive channels. *Annu. Rev. Biophys.* **39**, 111-137. doi:10.1146/annurev.biophys.37.032807.125836

Arnandis, T., Ferrer-Vicens, I., García-Trevijano, E. R., Miralles, V. J., García, C., Torres, L., Viña, J. R. and Zaragozá, R. (2012). Calpains mediate epithelial-cell death during mammary gland involution: mitochondria and lysosomal destabilization. *Cell Death Differ.* **19**, 1536-1548. doi:10.1038/cdd.2012.46

Babicki, S., Arndt, D., Marcu, A., Liang, Y., Grant, J. R., Maciejewski, A. and Wishart, D. S. (2016). Heatmapper: web-enabled heat mapping for all. *Nucleic Acids Res.* **44**, W147-W153. doi:10.1093/nar/gkw419

Bach, K., Pensa, S., Grzelak, M., Hadfield, J., Adams, D. J. J., Marioni, J. C. C. and Khaled, W. T. T. (2017). Differentiation dynamics of mammary epithelial cells revealed by single-cell RNA sequencing. *Nat. Commun.* **8**, 2128. doi:10.1038/s41467-017-02001-5

Bassett, J. J., Bong, A. H. L., Janke, E. K., Robitaille, M., Roberts-Thomson, S. J., Peters, A. A. and Monteith, G. R. (2018). Assessment of cytosolic free calcium changes during ceramide-induced cell death in MDA-MB-231 breast cancer cells expressing the calcium sensor GCaMP6m. *Cell Calcium* **72**, 39-50. doi:10.1016/j.ceca.2018.02.003

Beech, D. J. and Kalli, A. C. (2019). Force sensing by piezo channels in cardiovascular health and disease. *Arterioscler. Thromb. Vasc. Biol.* **39**, 2228-2239. doi:10.1161/ATVBAHA.119.313348

Bonnans, C., Chou, J. and Werb, Z. (2014). Remodelling the extracellular matrix in development and disease. *Nat. Rev. Mol. Cell Biol.* **15**, 786-801. doi:10.1038/nrm3904

Boulanger, J., Kervrann, C., Bouthemy, P., Elbau, P., Sibarita, J. B. and Salamero, J. (2010). Patch-based nonlocal functional for denoising fluorescence microscopy image sequences. *IEEE Trans. Med. Imaging* **29**, 442-454. doi:10.1109/TMI.2009.2033991

Bringmann, M. and Bergmann, D. C. (2017). Tissue-wide Mechanical Forces Influence the Polarity of Stomatal Stem Cells in Arabidopsis. *Curr. Biol.* **27**, 877-883. doi:10.1016/j.cub.2017.01.059

Brisken, C. and Ataca, D. (2015). Endocrine hormones and local signals during the development of the mouse mammary gland. *Wiley Interdiscip. Rev. Dev. Biol.* **4**, 181-195. doi:10.1002/wdev.172

Cahalan, S. M., Lukacs, V., Ranade, S. S., Chien, S., Bandell, M. and Patapoutian, A. (2015). Piezo1 links mechanical forces to red blood cell volume. *Elife* **4**, e07370. doi:10.7554/eLife.07370.013

Charras, G. and Yap, A. S. (2018). Tensile forces and mechanotransduction at cell–cell junctions. *Curr. Biol.* **28**, 445-457. doi:10.1016/j.cub.2018.02.003

Chen, T.-W., Wardill, T. J., Sun, Y., Pulver, S. R., Renninger, S. L., Baohan, A., Schreiter, E. R., Kerr, R. A., Orger, M. B., Jayaraman, V. et al. (2013). Ultrasensitive fluorescent proteins for imaging neuronal activity. *Nature* **499**, 295-300. doi:10.1038/nature12354

Coste, B., Mathur, J., Schmidt, M., Earley, T. J., Ranade, S., Petrus, M. J., Dubin, A. E. and Patapoutian, A. (2010). Piezo1 and Piezo2 are essential components of distinct mechanically activated cation channels. *Science (80-.)* **330**, 55-60. doi:10.1126/science.1193270

Davis, F. M. (2016). The ins and outs of calcium signalling in lactation and involution: implications for breast cancer treatment. *Pharmacol. Res.* **116**, 100-104. doi:10.1016/j.phrs.2016.12.007

Davis, F. M., Azimi, I., Faville, R. A., Peters, A. A., Jalink, K., Putney, J. W., Goodhill, G. J., Thompson, E. W., Roberts-Thomson, S. J. and Monteith, G. R. (2014). Induction of epithelial-mesenchymal transition (EMT) in breast cancer cells is calcium signal dependent. *Oncogene* **33**, 2307-2316. doi:10.1038/onc.2013.187

Davis, F. M., Janoshazi, A., Janardhan, K. S., Steinckwich, N., D'Agostin, D. M., Petranka, J. G., Desai, P. N., Roberts-Thomson, S. J., Bird, G. S., Tucker, D. K. et al. (2015). Essential role of Orai1 store-operated calcium channels in lactation. *Proc. Natl. Acad. Sci. USA* **112**, 5827-5832. doi:10.1073/pnas.1502264112

Davis, F. M., Lloyd-Lewis, B., Harris, O. B., Kozar, S., Winton, D. J., Muresan, L. and Watson, C. J. (2016). Single-cell lineage tracing in the mammary gland reveals stochastic clonal dispersion of stem/progenitor cell progeny. *Nat. Commun.* **7**, 13053. doi:10.1038/ncomms13053

Doppler, W., Groner, B. and Ball, R. K. (1989). Prolactin and glucocorticoid hormones synergistically induce expression of transfected rat beta-casein gene promoter constructs in a mammary epithelial cell line. *Proc. Natl. Acad. Sci USA* **86**, 104-108. doi:10.1073/pnas.86.1.104

dos Santos, C. O., Dolzhenko, E., Hodges, E., Smith, A. D. and Hannon, G. J. (2015). An epigenetic memory of pregnancy in the mouse mammary gland. *Cell Rep.* **11**, 1102-1109. doi:10.1016/j.celrep.2015.04.015

Eisenhoffer, G. T., Loftus, P. D., Yoshigi, M., Otsuna, H., Chien, C.-B., Morcos, P. A. and Rosenblatt, J. (2012). Crowding induces live cell extrusion to maintain homeostatic cell numbers in epithelia. *Nature* **484**, 546-549. doi:10.1038/nature10999

Fotiou, E., Martin-Almedina, S., Simpson, M. A., Lin, S., Gordon, K., Brice, G., Atton, G., Jeffery, I., Rees, D. C., Mignot, C. et al. (2015). Novel mutations in PIEZO1 cause an autosomal recessive generalized lymphatic dysplasia with non-immune hydrops fetalis. *Nat. Commun.* **6**, 8085. doi:10.1038/ncomms9085

Gimpl, G. and Fahrenholz, F. (2001). The oxytocin receptor system: structure, function, and regulation. *Physiol. Rev.* **81**, 629-683. doi:10.1152/physrev.2001.81.2.629

Gottlieb, P. A. (ed.) (2017). *Piezo Channels, Volume 79 (Current Topics in Membranes)*, 1st edn. Academic Press. pp 1-36. doi:10.1016/bs.ctm.2016.11.007

Gudipaty, S. A., Lindblom, J., Loftus, P. D., Redd, M. J., Edes, K., Davey, C. F., Krishnegowda, V. and Rosenblatt, J. (2017). Mechanical stretch triggers rapid epithelial cell division through Piezo1. *Nature* **543**, 118-121. doi:10.1038/nature21407

Haaksma, C. J., Schwartz, R. J. and Tomasek, J. J. (2011). Myoepithelial cell contraction and milk ejection are impaired in mammary glands of mice lacking smooth muscle alpha-actin. *Biol. Reprod.* **85**, 13-21. doi:10.1095/biolreprod.110.090639

Hughes, K. and Watson, C. J. (2018). Sinus-like dilatations of the mammary milk ducts, Ki67 expression, and CD3-positive T lymphocyte infiltration, in the mammary gland of wild European rabbits during pregnancy and lactation. *J. Anat.* **233**, 266-273. doi:10.1111/joa.12824

Hughes, K., Wickenden, J. A., Allen, J. E. and Watson, C. J. (2012). Conditional deletion of Stat3 in mammary epithelium impairs the acute phase response and modulates immune cell numbers during post-lactational regression. *J. Pathol.* **227**, 106-117. doi:10.1002/path.3961

Hynes, N. E. E., Taverna, D., Harwerth, I. M. M., Ciardiello, F., Salomon, D. S. S., Yamamoto, T. and Groner, B. (2015). Epidermal growth factor receptor, but not c-erbB-2, activation prevents lactogenic hormone induction of the beta-casein gene in mouse mammary epithelial cells. *Mol. Cell. Biol.* **10**, 4027-4034. doi:10.1128/MCB.10.8.4027

Ke, M.-T., Fujimoto, S. and Imai, T. (2013). SeeDB: a simple and morphology-preserving optical clearing agent for neuronal circuit reconstruction. *Nat. Neurosci.* **16**, 1154-1161. doi:10.1038/nn.3447

Kreuzaler, P. A., Staniszewska, A. D., Li, W., Omidvar, N., Kedjouar, B., Turkson, J., Poli, V., Flavell, R. A., Clarkson, R. W. E. and Watson, C. J. (2011). Stat3 controls lysosomal-mediated cell death in vivo. *Nat. Cell Biol.* **13**, 303-309. doi:10.1038/ncb2171

Kritikou, E. A., Sharkey, A., Abell, K., Came, P. J., Anderson, E., Clarkson, R. W. E. and Watson, C. J. (2003). A dual, non-redundant, role for LIF as a regulator of development and STAT3-mediated cell death in mammary gland. *Development* **130**, 3459-3468. doi:10.1242/dev.00578

Li, M., Liu, X., Robinson, G., Bar-Peled, U., Wagner, K.-U., Young, W. S., Hennighausen, L. and Furth, P. A. (2002). Mammary-derived signals activate programmed cell death during the first stage of mammary gland involution. *Proc. Natl. Acad. Sci. USA* **94**, 3425-3430

Li, J., Hou, B., Tumova, S., Muraki, K., Bruns, A., Ludlow, M. J., Sedo, A., Hyman, A. J., McKeown, L., Young, R. S. et al. (2014). Piezo1 integration of vascular architecture with physiological force. *Nature* **515**, 279-282. doi:10.1038/nature13701

Li, C., Rezania, S., Kammerer, S., Sokolowski, A., Devaney, T., Gorischek, A., Jahn, S., Hackl, H., Groschner, K., Windpassinger, C. et al. (2015). Piezo1 forms mechanosensitive ion channels in the human MCF-7 breast cancer cell line. *Sci. Rep.* **5**, 8364. doi:10.1038/srep08364

Linkert, M., Rueden, C. T., Allan, C., Burel, J.-M., Moore, W., Patterson, A., Loranger, B., Moore, J., Neves, C., MacDonald, D. et al. (2010). Metadata matters: access to image data in the real world. *J. Cell Biol.* **189**, 777-782. doi:10.1083/jcb.201004104

Lloyd-Lewis, B., Davis, F. M., Harris, O. B., Hitchcock, J. R., Lourenco, F. C., Pasche, M. and Watson, C. J. (2016). Imaging the mammary gland and

mammary tumours in 3D: Optical tissue clearing and immunofluorescence methods. *Breast Cancer Res.* **18**, 127. doi:10.1186/s13058-016-0754-9

Lloyd-Lewis, B., Harris, O. B., Watson, C. J. and Davis, F. M. (2017a). Mammary stem cells: premise, properties and perspectives. *Trends Cell Biol.* **8**, 556-567. doi:10.1016/j.tcb.2017.04.001

Lloyd-Lewis, B., Sargeant, T. J., Kreuzaler, P. A., Resemann, H. K., Pensa, S. and Watson, C. J. (2017b). Analysis of the involuting mouse mammary gland: an in vivo model for cell death. *Methods Mol. Biol.* **1501**, 165-186. doi:10.1007/978-1-4939-6475-8_7

Lloyd-Lewis, B., Davis, F. M., Harris, O. B., Hitchcock, J. R. and Watson, C. J. (2018). Neutral lineage tracing of proliferative embryonic and adultmammary stem/progenitor cells. *Development* **145**, 164079. doi:10.1242/dev.164079

Lund, L. R., Rømer, J., Thomasset, N., Solberg, H., Pyke, C., Bissell, M. J., Danø, K. and Werb, Z. (1996). Two distinct phases of apoptosis in mammary gland involution: proteinase-independent and -dependent pathways. *Development* **122**, 181-193.

Lyons, T. R., O′Brien, J., Borges, V. F., Conklin, M. W., Keely, P. J., Eliceiri, K. W., Marusyk, A., Tan, A.-C. and Schedin, P. (2011). Postpartum mammary gland involution drives progression of ductal carcinoma in situ through collagen and COX-2. *Nat. Med.* **17**, 1109-1115. doi:10.1038/nm.2416

Macias, H. and Hinck, L. (2012). Mammary gland development. *Wiley Interdiscip. Rev. Dev. Biol.* **1**, 533-557. doi:10.1002/wdev.35

Martinac, B. (2014). The ion channels to cytoskeleton connection as potential mechanism of mechanosensitivity. *Biochim. Biophys. Acta Biomembr* **1838**, 682-691. doi:10.1016/j.bbamem.2013.07.015

McAndrew, D., Grice, D. M. D. M., Peters, A. A. A. A., Davis, F. M. F. M., Stewart, T., Rice, M., Smart, C. E. C. E., Brown, M. A. M. A., Kenny, P. A. P. A., Roberts-Thomson, S. J. S. J. et al. (2011). ORAI1-mediated calcium influx in lactation and in breast cancer. *Mol. Cancer Ther.* **10**, 448-460. doi:10.1158/1535-7163.MCT-10-0923

McDaniel, S. M., Rumer, K. K., Biroc, S. L., Metz, R. P., Singh, M., Porter, W. and Schedin, P. (2006). Remodeling of the mammary microenvironment after lactation promotes breast tumor cell metastasis. *Am. J. Pathol.* **168**, 608-620. doi:10.2353/ajpath.2006.050677

McManaman, J. L. and Neville, M. C. (2003). Mammary physiology and milk secretion. *Adv. Drug Deliv. Rev.* **55**, 629-641. doi:10.1016/S0169-409X(03)00033-4

Meier-Abt, F., Brinkhaus, H. and Bentires-Alj, M. (2014). Early but not late pregnancy induces lifelong reductions in the proportion of mammary progesterone sensing cells and epithelial Wnt signaling. *Breast Cancer Res.* **16**, 402. doi:10.1186/bcr3626

Montalbetti, N., Dalghi, M. G., Albrecht, C. and Hediger, M. A. (2014). Nutrient transport in the mammary gland: Calcium, trace minerals and water soluble vitamins. *J. Mammary Gland Biol. Neoplasia* **19**, 73-90. doi:10.1007/s10911-014-9317-9

Nelson, C. M. and Bissell, M. J. (2006). Of extracellular matrix, scaffolds, and signaling: tissue architecture regulates development, homeostasis, and cancer. *Annu. Rev. Cell Dev. Biol.* **22**, 287-309. doi:10.1146/annurev.cellbio.22.010305.104315

Nonomura, K., Lukacs, V., Sweet, D., Goddard, L., Kanie, A., Whitwam, T., Ranade, S., Fujimori, T., Kahn, M. and Patapoutian, A. (2018). Mechanically activated ion channel PIEZO1 is required for lymphatic valve formation. *Proc. Natl. Acad. Sci. USA* **115**, 12817-12822. doi:10.1073/pnas.1817070115

Pan, B., Akyuz, N., Liu, X. P., Asai, Y., Nist-Lund, C., Kurima, K., Derfler, B. H., György, B., Limapichat, W., Walujkar, S. et al. (2018). TMC1 forms the pore of mechanosensory transduction channels in vertebrate inner ear hair cells. *Neuron* **99**, 736-753.e6. doi:10.1016/j.neuron.2018.07.033

Pidhorskyi, S., Morehead, M., Jones, Q., Spirou, G. and Doretto, G. (2018). syGlass: Interactive Exploration of Multidimensional Images Using Virtual Reality Head-mounted Displays. *arXiv* https://arxiv.org/abs/1804.08197

Pitelka, D. R., Hamamoto, S. T., Duafala, J. G. and Nemanic, M. K. (1973). Cell contacts in the mouse mammary gland I. Normal gland in postnatal development and the secretory cycle. *J. Cell Biol.* **56**, 797-818. doi:10.1083/jcb.56.3.797

Prater, M., Shehata, M., Watson, C. J. and Stingl, J. (2013). Enzymatic dissociation, flow cytometric analysis, and culture of normal mouse mammary tissue. *Methods Mol. Biol.* **946**, 395-409. doi:10.1007/978-1-62703-128-8_25

Provenzano, P. P., Inman, D. R., Eliceiri, K. W. and Keely, P. J. (2009). Matrix density-induced mechanoregulation of breast cell phenotype, signaling and gene expression through a FAK-ERK linkage. *Oncogene* **28**, 4326-4343. doi:10.1038/onc.2009.299

Quaglino, A., Salierno, M., Pellegrotti, J., Rubinstein, N. and Kordon, E. C. (2009). Mechanical strain induces involution-associated events in mammary epithelial cells. *BMC Cell Biol.* **10**, 55. doi:10.1186/1471-2121-10-55

Ranade, S. S., Woo, S. H., Dubin, A. E., Moshourab, R. A., Wetzel, C., Petrus, M., Mathur, J., Bégay, V., Coste, B., Mainquist, J. et al. (2014). Piezo2 is the major transducer of mechanical forces for touch sensation in mice. *Nature* **516**, 121-125. doi:10.1038/nature13980

Raymond, K., Cagnet, S., Kreft, M., Janssen, H., Sonnenberg, A. and Glukhova, M. A. (2011). Control of mammary myoepithelial cell contractile function by α3β1 integrin signalling. *EMBO J.* **30**, 1896-1906. doi:10.1038/emboj.2011.113

Reinhardt, T. A. and Horst, R. L. (1999). Ca2+-ATPases and their expression in the mammary gland of pregnant and lactating rats. *Am. J. Physiol.* **276**, C796-C802. doi:10.1152/ajpcell.1999.276.4.C796

Rios, A. C., Fu, N. Y., Lindeman, G. J. and Visvader, J. E. (2014). In situ identification of bipotent stem cells in the mammary gland. *Nature* **506**, 322-327. doi:10.1038/nature12948

Romac, J. M. J., Shahid, R. A., Swain, S. M., Vigna, S. R. and Liddle, R. A. (2018). Piezo1 is a mechanically activated ion channel and mediates pressure induced pancreatitis. *Nat. Commun.* **9**, 1715. doi:10.1038/s41467-018-04194-9

Rudolf, R., Magalhães, P. J. and Pozzan, T. (2006). Direct in vivo monitoring of sarcoplasmic reticulum Ca2+ and cytosolic cAMP dynamics in mouse skeletal muscle. *J. Cell Biol.* **173**, 187-193. doi:10.1083/jcb.200601160

Sargeant, T. J., Lloyd-Lewis, B., Resemann, H. K., Ramos-Montoya, A., Skepper, J. and Watson, C. J. (2014). Stat3 controls cell death during mammary gland involution by regulating uptake of milk fat globules and lysosomal membrane permeabilization. *Nat. Cell Biol.* **16**, 1057-1068. doi:10.1038/ncb3043

Schedin, P. and Keely, P. J. (2011). Mammary gland ECM remodeling, stiffness, and mechanosignaling in normal development and tumor progression. *Cold Spring Harb. Perspect. Biol.* **3**, a003228. doi:10.1101/cshperspect.a003228

Schedin, P., Mitrenga, T., McDaniel, S. and Kaeck, M. (2004). Mammary ECM Composition and function are altered by reproductive state. *Mol. Carcinog.* **41**, 207-220. doi:10.1002/mc.20058

Scheele, C. L. G. J., Hannezo, E., Muraro, M. J., Zomer, A., Langedijk, N. S. M., van Oudenaarden, A., Simons, B. D. and van Rheenen, J. (2017). Identity and dynamics of mammary stem cells during branching morphogenesis. *Nature* **542**, 313-317. doi:10.1038/nature21046

Schindelin, J., Arganda-Carreras, I., Frise, E., Kaynig, V., Longair, M., Pietzsch, T., Preibisch, S., Rueden, C., Saalfeld, S., Schmid, B. et al. (2012). Fiji: an open source platform for biological image analysis. *Nat. Methods* **9**, 676-682. doi:10.1038/nmeth.2019

Schwartz, M. A. (2010). Integrins and extracellular matrix in mechanotransduction. *Cold Spring Harb. Perspect. Biol.* **25**, 613-618. doi:10.1101/cshperspect.a005066

Servin-Vences, M. R., Moroni, M., Lewin, G. R. and Poole, K. (2017). Direct measurement of TRPV4 and PIEZO1 activity reveals multiple mechanotransduction pathways in chondrocytes. *Elife* **6**, e21074. doi:10.7554/eLife.21074

Sherman, M. E., Figueroa, J. D., Henry, J. E., Clare, S. E., Rufenbarger, C. and Storniolo, A. M. (2012). The Susan G. Komen for the cure tissue bank at the IU simon cancer center: a unique resource for defining the “molecular histology” of the breast. *Cancer Prev. Res.* **5**, 528-535. doi:10.1158/1940-6207.CAPR-11-0234

Slepicka, P. F., Cyrill, S. L. and dos Santos, C. O. (2019). Pregnancy and Breast Cancer: Pathways to Understand Risk and Prevention. *Trends Mol. Med.* **25**, 866-881. doi:10.1016/j.molmed.2019.06.003

Sommer, C., Straehle, C., Kothe, U. and Hamprecht, F. A. (2011). Ilastik: Interactive learning and segmentation toolkit. In Proceedings - International Symposium on Biomedical Imaging. doi:10.1038/s41592-019-0582-9

Sreekumar, A., Toneff, M. J., Toh, E., Roarty, K., Creighton, C. J., Belka, G. K., Lee, D.-K., Xu, J., Chodosh, L. A., Richards, J. S. et al. (2017). WNT-mediated regulation of FOXO1 constitutes a critical axis maintaining pubertal mammary stem cell homeostasis. *Dev. Cell* **43**, 436-448. doi:10.1016/j.devcel.2017.10.007

Stein, T., Salomonis, N. and Gusterson, B. A. (2007). Mammary gland involution as a multi-step process. *J. Mammary Gland Biol. Neoplasia* **12**, 25-35. doi:10.1007/s10911-007-9035-7

Stevens, C. and Hunter, P. J. (2003). Sarcomere length changes in a 3D mathematical model of the pig ventricles. *Prog. Biophys. Mol. Biol.* **82**, 229-241. doi:10.1016/S0079-6107(03)00023-3

Stevenson, A. J., Vanwalleghem, G., Stewart, T. A., Condon, N. D., Lloyd-Lewis, B., Marino, N., Putney, J. W., Scott, E. K., Ewing, A. D. and Davis, F. M. (2020). Multiscale imaging of basal cell dynamics in the functionally mature mammary gland. *Proc. Natl. Acad. Sci. USA* **117**, 26822-26832. doi:10.1073/pnas.2016905117

Stewart, T. A. and Davis, F. M. (2019a). Formation and function of mammalian epithelia: roles for mechanosensitive PIEZO1 ion channels. *Front. Cell Dev. Biol.* **7**, 260. doi:10.3389/fcell.2019.00260

Stewart, T. A. and Davis, F. M. (2019b). A primary cell and organoid platform for evaluating pharmacological responses in mammary epithelial cells. *ACS Pharmacol. Transl. Sci.* **3**, 63-75. doi:10.1021/acsptsci.9b00090

Stewart, T. A. and Davis, F. M. (2020). Got milk? Identifying and characterizing lactation defects in genetically-engineered mouse models. *J. Mammary Gland Biol. Neoplasia*. doi:10.1007/s10911-020-09467-y

Suchanek, K. M., May, F. J., Robinson, J. A., Lee, W. J., Holman, N. A., Monteith, G. R. and Roberts-Thomson, S. J. (2002). Peroxisome proliferator-activated receptor alpha in the human breast cancer cell lines MCF-7 and MDA-MB-231. *Mol. Carcinog.* **34**, 165-171. doi:10.1002/mc.10061

Susaki, E. A. A. and Ueda, H. R. R. (2016). Whole-body and whole-organ clearing and imaging techniques with single-cell resolution: toward organism-level systems biology in mammals. *Cell Chem. Biol.* **23**, 137-157. doi:10.1016/j.chembiol.2015.11.009

Syeda, R., Xu, J., Dubin, A. E., Coste, B., Mathur, J., Huynh, T., Matzen, J., Lao, J., Tully, D. C., Engels, I. H. et al. (2015). Chemical activation of the mechanotransduction channel Piezo1. *Elife* **4**, e07369. doi:10.7554/eLife.07369

Thévenaz, P., Ruttimann, U. E. and Unser, M. (1998). A pyramid approach to subpixel registration based on intensity. *IEEE Trans. Image Process* **7**, 27-41. doi:10.1109/83.650848

Tokita, Y., Akiho, H., Nakamura, K., Ihara, E. and Yamamoto, M. (2015). Contraction of gut smooth muscle cells assessed by fluorescence imaging. *J. Pharmacol. Sci.* **127**, 344-351. doi:10.1016/j.jphs.2015.02.002

Tse, J. M., Cheng, G., Tyrrell, J. A., Wilcox-Adelman, S. A., Boucher, Y., Jain, R. K. and Munn, L. L. (2012). Mechanical compression drives cancer cells toward invasive phenotype. *Proc. Natl. Acad. Sci. USA* **109**, 911-916. doi:10.1073/pnas.1118910109

Tsuchiya, M., Hara, Y., Okuda, M., Itoh, K., Nishioka, R., Shiomi, A., Nagao, K., Mori, M., Mori, Y., Ikenouchi, J. et al. (2018). Cell surface flip-flop of phosphatidylserine is critical for PIEZO1-mediated myotube formation. *Nat. Commun.* **9**, 2049. doi:10.1038/s41467-018-04436-w

Tuthill, J. C. and Wilson, R. I. (2016). Mechanosensation and adaptive motor control in insects. *Curr. Biol.* **26**, 1022-1038. doi:10.1016/j.cub.2016.06.070

VanHouten, J., Sullivan, C., Bazinet, C., Ryoo, T., Camp, R., Rimm, D. L., Chung, G. and Wysolmerski, J. (2010). PMCA2 regulates apoptosis during mammary gland involution and predicts outcome in breast cancer. *Proc. Natl. Acad. Sci. USA* **107**, 11405-11410. doi:10.1073/pnas.0911186107

Van Keymeulen, A., Rocha, A. S., Ousset, M., Beck, B., Bouvencourt, G., Rock, J., Sharma, N., Dekoninck, S. and Blanpain, C. (2011). Distinct stem cells contribute to mammary gland development and maintenance. *Nature* **479**, 189-193. doi:10.1038/nature10573

Van Keymeulen, A., Fioramonti, M., Centonze, A., Bouvencourt, G., Achouri, Y. and Blanpain, C. (2017). Lineage-restricted mammary stem cells sustain the development, homeostasis, and regeneration of the estrogen receptor positive lineage. *Cell Rep.* **20**, 1525-1532. doi:10.1016/j.celrep.2017.07.066

Wagner, K. U., Wall, R. J., St-Onge, L., Gruss, P., Wynshaw-Boris, A., Garrett, L., Li, M., Furth, P. A. and Hennighausen, L. (1997). Cre-mediated gene deletion in the mammary gland. *Nucleic Acids Res.* **25**, 4323-4330. doi:10.1093/nar/25.21.4323

Watson, C. J. (2006). Key stages in mammary gland development Involution: apoptosis and tissue remodelling that convert the mammary gland from milk factory to a quiescent organ. *Breast Cancer Res.* **8**, 203. doi:10.1186/bcr1401

Watson, C. J. and Kreuzaler, P. A. (2011). Remodeling mechanisms of the mammary gland during involution. *Int. J. Dev. Biol.* **55**, 757-762. doi:10.1387/ijdb.113414cw

Webb, R. and Schieber, N. (2018). Volume scanning electron microscopy: serial block-face scanning electron microscopy focussed ion beam scanning electron microscopy. In *Cellular Imaging. Biological and Medical Physics, Biomedical Engineering* (ed. E. Hanssen), pp. 117-148. Cham: Springer.

Woo, S. H., Lukacs, V., De Nooij, J. C., Zaytseva, D., Criddle, C. R., Francisco, A., Jessell, T. M., Wilkinson, K. A. and Patapoutian, A. (2015). Piezo2 is the principal mechanotransduction channel for proprioception. *Nat. Neurosci.* **18**, 1756-1762. doi:10.1038/nn.4162

Xing, J., Petranka, J. G. J. G., Davis, F. M. F. M., Desai, P. N. P. N., Putney, J. W. J. W. and Bird, G. S. G. S. (2014). Role of Orai1 and store-operated calcium entry in mouse lacrimal gland signalling and function. *J. Physiol.* **592**, 927-939. doi:10.1113/jphysiol.2013.267740

Xu, J., Mathur, J., Vessières, E., Hammack, S., Nonomura, K., Favre, J., Grimaud, L., Petrus, M., Francisco, A., Li, J. et al. (2018). GRP68 senses flow and is essential for vascular physiology. *Cell* **173**, 762-775. doi:10.1016/j.cell.2018.03.076

Zeng, W. Z., Marshall, K. L., Min, S., Daou, I., Chapleau, M. W., Abboud, F. M., Liberles, S. D. and Patapoutian, A. (2018). PIEZOs mediate neuronal sensing of blood pressure and the baroreceptor reflex. *Science (80-.)* **362**, 464-467. doi:10.1126/science.aau6324

Zwick, R. K., Rudolph, M. C., Shook, B. A., Holtrup, B., Roth, E., Lei, V., Van Keymeulen, A., Seewaldt, V., Kwei, S., Wysolmerski, J. et al. (2018). Adipocyte hypertrophy and lipid dynamics underlie mammary gland remodeling after lactation. *Nat. Commun.* **9**, 3592. doi:10.1038/s41467-018-05911-0